The mRNA covalent modification dihydrouridine regulates transcript turnover and photosynthetic capacity during plant abiotic stress

Li'ang Yu[1], Giovanni Melandri[2,3], Anna C. Nelson Dittrich[1], Sebastian Calleja[2], Diep R. Ganguly[4], Kyle Palos[1], Emily K. Brewer[1], Hillary Fischer[5], Bruno Rozzi[2], Aparna Srinivasan[1], Toshihiro Obata[6], Hamada Abd Elgawad[7], Gerrit T.S. Beemster[7], Riley Henderson[1], Ciara Denise Garcia[2], Xiaodan Zhang[1], David Stern[1], Andrea Eveland[8], Eric Lyons[2], A. Elizabeth Arnold[2,3], Aleksandra Skirycz[5], Susan J. Schroeder[9], Brian D. Gregory[4]*, Duke Pauli[2,3]*, Andrew D. L. Nelson[1]*

[1]Boyce Thompson Institute, Cornell University, Ithaca, NY 14850, USA
[2]School of Plant Sciences, University of Arizona, Tucson, AZ, 85721, USA
[3]Center for Agroecosystem Research in the Desert (ARID), University of Arizona, Tucson, AZ 85721, USA
[4]Department of Biology, University of Pennsylvania, Philadelphia, PA, USA
[5]Department of Biochemistry and Molecular Biology, Michigan State University, East Lansing, MI, 48824, USA
[6]Department of Biochemistry and Center for Plant Science Innovation, University of Nebraska-Lincoln, NE, 68588, USA
[7]Integrated Molecular Plant Physiology Research, University of Antwerp, 2020 Antwerp, Belgium
[8]Donald Danforth Plant Science Center, St. Louis, MO, 63132, USA
[9]Department of Chemistry and Biochemistry, The University of Oklahoma, Norman, OK, 73019, USA

***Address correspondence to:**
Dr. Andrew D. L. Nelson
The Boyce Thompson Institute, Cornell University
533 Tower Road, Ithaca, NY, 14850.
an425@cornell.edu

or
Dr. Duke Pauli
The University of Arizona, School of Plant Sciences
1140 E. South Campus Drive, Tucson, AZ, 85721
dukepauli@arizona.edu

or
Dr. Brian D. Gregory
University of Pennsylvania, Department of Biology, 103 H Lynch Laboratory
433 South University Avenue, Philadelphia, PA, 19104
bdgregor@sas.upenn.edu

Current Email addresses:
LY: ly76@cornell.edu, GM: gmelandri@arizona.edu, ACND: an426@cornell.edu, SC: scalleja@arizona.edu, DRG: dganguly@sas.upenn.edu, KP: kpalos001@gmail.com, EKB: emilybrewer@unr.edu, HF: fisch333@msu.edu, BR: brozzi@ufl.edu, ApS: aparna3@outlook.com,TO: tobata2@unl.edu, HAE: hamada.abdelgawad@uantwerp.be, GTSB: gerrit.beemster@uantwerp.be, RH: rnh53@cornell.edu, CDG: ciarag@arizona.edu, XZ: xiaodanz091391@gmail.com, DS: ds28@cornell.edu, AE: AEveland@danforthcenter.org, SJS: susan.schroeder@ou.edu, AIS: skirycza@msu.edu, EL: ericlyons@arizona.edu, AEA: barnoldaz@gmail.com

Running title: The RCM Dihydrouridine impacts mRNA turnover and abiotic stress resilience

Abstract

RNA Covalent Modifications (RCMs) are post-transcriptional chemical alterations that influence RNA stability and translation efficiency, thus play critical roles in eukaryotic growth and development. However, their role in regulating plant performance under abiotic stress remain largely unexplored. Here, we integrated multi-omics data in six *Sorghum bicolor* accessions under water-limiting conditions in the field to explore the relationship between RCMs and drought response. Within a stress and photosynthesis-associated gene co-expression module, we identified *SbDUS2*, a member of family of enzymes, conserved across eukaryotes, which catalyzes the reduction of uracil to dihydrouridine (DHU) on RNA molecules. DHU-modified transcripts in this module were enriched for photosynthetic functions and showed strong correlation with photosynthetic traits. To elucidate the function of this RCM, we characterized loss of function *dus2* mutants in the genetic model, *Arabidopsis thaliana*. Under control conditions, these DHU-deficient mutants exhibited impaired germination and delayed development. Furthermore, when exposed to heat or water-limiting conditions, these mutants showed significantly reduced net CO_2 assimilation and survival. Using multiple transcriptome-wide RNA stability assays, we demonstrated that transcripts associated with lower DHU level in a *dus2* background generally exhibited increased stability compared to Col-0 controls. Particularly, lack of DUS2 led to the hyperstability of photosynthesis-related transcripts, impeding their turnover and likely preventing proper photosynthetic acclimation during stress. We propose a model based on these data where DHU acts as a critical post-transcriptional regulator marking mRNAs for rapid turnover under stress, highlighting an overlooked regulatory layer contributing to plant resilience.

Keywords:

Abiotic stress response, mRNA dihydrouridylation, Systems biology, Photosynthesis, Epitranscriptome, RNA modification

Introduction

Agricultural production faces intensifying challenges as drought and heat stressors increase in frequency and severity across major cropping regions (Alizadeh et al., 2020). These abiotic stressors trigger a range of adverse phenotypic and physiological responses, including heightened susceptibility to biotic stresses, altered development, and reduced yield. Consequently, enhancing plant productivity and resilience under such conditions has become a primary goal in improving stress tolerance. A widely adopted strategy to achieve this goal involves the exploration and utilization of genetic variation (Glaszmann et al., 2010; Khoury et al., 2022). While large population-level studies within many crop species have identified strong abiotic stress tolerance phenotypes and associated loci useful for breeding and selection (Gilliham et al., 2017), the crosstalk between many upstream regulatory genes and downstream trait-associated genes remains unclear and largely unexplored. In addition to feedback at the DNA, RNA, and protein level, there are additional levels of regulatory control that make identifying beneficial alleles for crop improvement more challenging.

RNAs endure numerous co- and post-transcriptional events that influence their function, one of which is the covalent modification, or isomerization, of RNA bases. RNA covalent modifications (RCMs) are an emerging and underexplored layer of regulation in eukaryotes (Harcourt et al., 2017; Roundtree et al., 2017). RCMs are widespread and chemically diverse, decorating all classes of RNA, non-coding and coding alike (Finet et al., 2022a). As a natural result of their higher abundance, most RCMs were first characterized on housekeeping RNAs such as tRNAs and rRNAs (Yu et al., 2011; Toubdji et al., 2024). One such RCM is dihydrouridine (DHU), which is formed by the reduction of the double bond in uridine by a highly conserved class of dihydrouridine synthase (DUS) enzymes (Yu et al., 2011). DHU is known to disrupt base stacking and increase RNA flexibility, particularly in tRNAs, where it is critical for the formation of the D-loop (Toubdji et al., 2024), a role that is conserved across all living organisms (Lombard et al., 2022). In non-plant systems, DHU has recently been found in mRNAs, predominantly in transcripts associated with core cellular mechanisms (Kato et al., 2005; Rider et al., 2009; Finet et al., 2022b). Disruption or depletion of DHU from these transcripts results in growth defects in yeast and, in humans, enhanced tumorigenesis (Kato et al., 2005; Rider et al., 2009). Despite the growing evidence that DHU plays an important role in mRNAs, how DHU regulates mRNA function, and the extent to which this RCM is present in plant mRNAs, is unclear.

Much of what we know about mRNA-associated RCMs comes from studies on N6-methyladenosine (m^6A), which has been shown to influence plant development and stress responses by modulating mRNA fate (Zhou et al., 2022; Shao et al., 2025; Liu et al., 2025). RCMs are known to regulate RNA stability, structure, translation, and localization within, and potentially between, cells (Arribas-

106 Hernández et al., 2018; Anderson et al., 2018; Luo et al., 2020; Cheng et al., 2021; Prall et al., 2023).
107 Despite this growing appreciation of the roles that RCMs can perform, many evolutionarily conserved
108 RCMs, such as DHU, pseudouridine (Ψ), N^1-methyladenosine (m^1A), and 5-methylcytidine (m^5C), remain
109 largely unknown in plants (Tang et al., 2020; Yang et al., 2020; Li et al., 2025). This knowledge gap stems
110 in part from technical barriers. Several RCMs can be detected with antibody-based methods (Dominissini
111 et al., 2012; Meyer et al., 2012; Edelheit et al., 2013; Li et al., 2016), and more recently at the transcript
112 level using Oxford Nanopore direct RNA-seq (DRS) along with trained algorithms to detect specific
113 modified ribonucleotides (Garalde et al., 2018; Liu et al., 2019; LaPierre et al., 2019; Wu et al., 2024;
114 Cruciani et al., 2025). For modifications that impact the base-pairing edge, bioinformatic approaches that
115 interpret the pattern of resulting RT-induced errors at modified sites have been deployed with great
116 success (Ryvkin et al., 2013; Tan et al., 2021). Although somewhat limited in resolution (Helm and
117 Motorin, 2017), these approaches have nevertheless been helpful in extending insights into the roles of
118 less studied RCMs (Sharma et al., 2023).

119 Sorghum [*Sorghum bicolor* (L.) Moench] is a heat- and drought-tolerant crop widely cultivated for
120 grain, forage, and cellulosic biomass production (Lobell et al., 2008; Abreha et al., 2021). Due to its
121 phylogenetic placement within the *Poaceae*, findings from sorghum often transfer to other critical
122 agronomic crops such as *Zea mays*. A well annotated genome (McCormick et al., 2018), along with the
123 physiological and morphological variation found within multiple diversity panels (Morris et al., 2013; Wu
124 et al., 2022; Boatwright et al., 2022), make sorghum ideal for supporting comparative, systems-level
125 analyses on field-grown plants. Indeed, several studies have used these resources to highlight
126 transcriptional responses to heat and drought stress in sorghum, uncovering genetic factors that might
127 contribute to improved stress resilience in sorghum and other important grasses (Boyles et al., 2019;
128 Varoquaux et al., 2019). Thus, these resources and characteristics make sorghum ideally suited for
129 uncovering RNA-based regulatory mechanisms contributing to plant resilience.

130 Here we leveraged a systems biology approach to study how six phylogenetically distinct sorghum
131 accessions with different levels of drought tolerance respond to water limiting conditions over time. Our
132 integrative approach using global-wide datasets identified the transcripts with DHU modification and its
133 corresponding enzyme for DHU synthesis in sorghum, SbDUS2, as strongly associated with plant
134 photosynthetic performance in the field. Interestingly, SbDUS2 is orthologous to human and fission yeast
135 DUS2, which were both previously found to be responsible for mRNA DHU deposition. Given the deeply
136 conserved nature of the DUS enzymes, we turned to *Arabidopsis thaliana*, where genetic *loss-of-function*
137 mutants for the orthologous DUS2 were available, to investigate the functional role of DHU in *Arabidopsis*.
138 Under control conditions, *Atdus2* mutants displayed reduced germination and delayed growth relative to
139 *AtDus2* controls. A set of complementary approaches were used to confirm that Arabidopsis *dus2*

140 mutants displayed reduced DHU levels, particularly on mRNAs associated with photosynthesis and
141 metabolism. After confirming that *Atdus2* mutants displayed reduced DHU levels on mRNAs, we used
142 this background to better understand the role of DHU in plant stress responses. Interestingly, *Atdus2*
143 mutants exhibited a similar physiological response to drought and heat, showing reduced CO_2
144 assimilation and lower survival. In Col-0 controls under heat, but not in the *Atdus2* background,
145 photosynthesis-related transcripts were found to be differentially DHU modified, a phenomenon that
146 coincided with decreased abundance for the associated transcripts. Using transcriptional arrest time
147 course-derived RNA decay assay at global level, we demonstrated that DHU predominantly destabilizes
148 mRNAs under control and abiotic stress conditions in Arabidopsis, and propose a model whereby DHU
149 is critical for mRNA turnover, particularly under stress scenarios, highlighting the significance of this
150 overlooked regulatory mechanisms with real-world agronomic relevance.
151

152 ## Methods and Materials

153 ### *Sorghum growth and phenotypic measurement*

154 Six selected sorghum accessions (PI 533871: M1, PI 533961: DL/59/1530, PI 656041: 80M, PI
155 656053: N290-B, PI 656076: SC1271, and PI 656096: SC391) were grown at the University of Arizona
156 Maricopa Agricultural Center (MAC). All plants were well-watered (WW) at the same rate (~24% soil
157 volume metric water content, SVWC), corresponding approximately to the soil field capacity) until flag
158 leaf appearance in the whorl (~47 days after planting), after which irrigation was reduced to a subset of
159 plots to mimic drought treatment (water-limited, WL; 16% SVWC). The destructive plant phenotyping was
160 conducted at the end of the season (maturity stage). Measured traits included above-ground biomass,
161 root biomass, and three-leaf weights. For other time-series molecular phenotypes, samples were
162 collected weekly (on Thursdays) for seven weeks (week 1-week 7, from August 13th to September 24th,
163 2020) on a specific range of a large field experiment conducted at the University of Arizona's Maricopa
164 Agricultural Center (MAC). For transcriptomics, metabolomics, and analysis of other biochemical traits,
165 samples consisting of six leaf disks from five different plants per accession, treatment, and time point
166 were collected (from 10:30 to 11:30) in three different 1.5 mL tubes and immediately snap-frozen in liquid
167 nitrogen. LI-6800 derived photosynthesis-related traits (N = 29, LI-COR Lincoln, NE) were measured in
168 the morning (from 9:00 to 10:00) and afternoon (from 13:00 to 14:00) with the following settings: Flow
169 rate = 600 μmol s^{-1}; Mixing fan speed =12,000 rpm; CO_2 = 420 ppm; Light= 2,000 μmol m^{-2} s^{-1}. The
170 youngest fully expanded leaf on the main stem of each plant was selected for the measurements and
171 data were logged as soon as assimilation and stomatal conductance curves (monitored in real-time on
172 the instrument display) when reaching a plateau (on average 30 seconds after a leaf was clamped).

173 ***Sorghum biochemical trait measurements***

174 Highly concentrated metabolites (e.g., total soluble sugars), levels of oxidative stress markers
175 and molecular antioxidants, and antioxidant enzyme and photorespiration enzyme activities were
176 analyzed using existing protocol (Melandri et al., 2020). Chlorophyll and carotenoid contents were
177 measured after acetone extraction (Porra et al., 1989). Sugar levels were quantified using enzyme-
178 coupled assays (Riewe et al., 2012). Oxidative stress markers, such as malondialdehyde (MDA) and
179 protein carbonyl content, were measured to assess lipid peroxidation and protein oxidation (Levine et al.,
180 1994; Hodges et al., 1999). Photorespiration-related enzyme activities, glycolate oxidase (GOX) and
181 hydroxypyruvate reductase (HPR), were assessed based on established methodologies (Feierabend and
182 Beevers, 1972; Schwitzguebel and Siegenthaler, 1984). Lipoxygenase (LOX) was extracted in potassium
183 phosphate buffer (pH 7.0), and its activity was measured by changes in conjugated dienes. Total
184 antioxidant capacity (TAC), total polyphenol content (Poly), and flavonoids were evaluated using standard
185 spectrophotometric assays (Benzie and Strain, 1999; Zhang et al., 2006). Enzyme activities of key
186 antioxidants, including ascorbate peroxidase (APX), dehydroascorbate reductase (DHAR),
187 monodehydroascorbate reductase (MDHAR), glutathione reductase (GR), peroxidase (POX), superoxide
188 dismutase (SOD), glutathione peroxidase (GPX), catalase (CAT), ascorbate oxidase (AO), and
189 glutathione *S*-transferase (GST), were determined using microplate-based kinetic assays (Aebi, 1984;
190 Murshed et al., 2008).

191

192 ***Sorghum metabolite profiling***

193 Primary sorghum metabolites were quantified using gas chromatography-mass spectrometry
194 (GC-MS, (Wase et al., 2022). Briefly, metabolites were extracted by methanol: water: chloroform solution
195 from 30±3 mg fresh weight (FW) of frozen samples. Ribitol was added to the extraction solution as internal
196 standard (IS). Dried metabolites were derivatized by methoxyamination and trimethylsylilation and
197 analyzed by a 7200 GC-QTOF system (Agilent, St Clara, CA, USA) using a HP-5MS-UI column (30 m
198 0.25 mm ID 0.25 µm; Agilent) with 100 x split and splitless modes. Metabolite peaks were annotated by
199 MassHunter Anaysis (Agilent) using the Fiehn Metabolomics Library (Agilent). The 42 most confidently
200 annotated metabolites were quantified by MassHunter Quantitation (Agilent) and the peak heights were
201 background subtracted, normalized by IS and precise fresh weight of the sample to calculate the relative
202 metabolite contents values.

203

204 ***General characterization of the Arabidopsis dus2 mutants***

205 Arabidopsis Col-0 and *dus2* mutant lines (Line ID: CS857388 and SALK_063052C,
206 https://abrc.osu.edu) were grown under standard Arabidopsis long-day conditions unless otherwise

207 specified (22°C, 60% humidity, and 16h light, 8h dark). All seeds were stratified at 4°C for 48~72 hours
208 prior to planting. T-DNA insertions were confirmed by PCR using primers designed from Salk T-DNA
209 Express (http://signal.salk.edu/tdnaprimers.2.html; SALK_063052: 5'- GATTGAGCTGGAACGTCTCAC
210 - 3', 3'- AGCAGAATCTGAGAACCAAATG -5'; CS857388: 5'-ACGCTCTCTTTCAGGATGTTG-3', 3'-
211 GCTGGTACACCAAGTTTCTCG-5'; L4 primer: 5'-TGATCCATGTAGATTTCCCGGACATGAAG-3').
212 PCR was performed for 40 cycles with an annealing temperature of 56°C. Germination assays were
213 performed on ½ MS medium with Col-0 and *dus2* mutant seeds at 22°C during each 3-hour interval for
214 27 hours after seed stratification (Murashige and Skoog, 1962). Two weeks after germination, Col-0 and
215 *dus2* two mutant accessions were divided into separate batches for plant growth rate (kept under long
216 day conditions) and photosynthetic measurements (shifted to a short-day chamber). Four weeks after
217 germination, treatments were applied.
218

219 ***Measuring impact of abiotic stress on growth rates of Arabidopsis dus2 mutants***

220 Col-0 and two *dus2* mutant lines (CS857388 and SALK_063052C) were used for abiotic stress
221 experiments. Drought treatment occurred at 22°C, with soil water content (SWC) held at 70% for control
222 and 25% for drought set, and lighting period: 8:00 - 21:00 for three days on four-week-old seedlings. Leaf
223 area measurements were performed using RGB imagery after a 3-day water withholding period on plant
224 rosettes using the PlantCV pipeline for trait extraction (Fahlgren et al., 2015). Heat treatment was
225 performed at 37°C for plants grown on soil and media plate. For soil seedlings, 2-week-old seedlings
226 were placed under 22°C and 37°C conditions over 12 days. Plant time-series biomass profiling under
227 these two conditions were performed using Raspi-controlled phenotyping tools (Pheno-Rigs, (Yu et al.,
228 2024a) to collect time-series plant RGB images (imaging-interval: 30 mins**,** length: 12 days) with
229 quantification of digital biomass of using PlantCV pipelines. For media plate seedlings, 7-day-old young
230 seedling were placed under 22°C and 37°C conditions over 72 hours for observation of seedling color
231 with images.
232

233 ***Measuring photosynthetic efficiency in Arabidopsis dus2 mutants under abiotic stress***

234 The photosynthetic efficiency of *dus2* and Col-0 lines was evaluated using a gas exchange
235 approach with the LI-6800 (LI-COR Lincoln, NE). Briefly, plants were maintained under short-day (SD)
236 growth conditions (photoperiod: 8:00-17:00, temp: 22°C) to enlarge rosette area to cover the 2cm^2 small
237 chamber of the LI-6800 device (Brazel et al., 2025). After 4-weeks, plants were kept at 22°C(control),
238 heat (37°C for 24 hours), and drought (25% SWC for 24 hours) for gas exchange measurement.
239 Parameters were set as follows: Flow rate = 400 μmol s^{-1}, Relative humidity of air = 55–60 %, Reference
240 CO_2 = 400 μmol^{-1}, Mixing fan speed = 10,000 rpm, Heat exchanger temperature: 22°C or 37°C, Chamber

241 pressure = 0.2 kPa, Light source composition 90 % red 10 % blue light, Light intensity = 1000 μmol m^{-2} s^{-1},
242 Measurement time = between 12:00 and 14:00 (Brazel et al., 2025).
243
244 ***RNA extraction and library construction***
245 RNA extraction was performed using methods from previous studies for both Arabidopsis and
246 sorghum (Burgess, 2023). Approximately five flash-frozen ¼ inch sorghum leaf disks per sample were
247 used as starting material for RNA extractions. RNA extraction was performed using the RNeasy Plant
248 Mini kit (Qiagen #74904) and RNase-free DNase set (Qiagen #79254). Approximately 2.5-10 ug total
249 RNA was used as starting material for mRNA enrichment using the Dynabeads mRNA purification kit
250 (Invitrogen #61006), except with the addition of a second binding and elution step to further enrich mRNA.
251 RNA-seq libraries were then constructed from 10-60 ng mRNA per sample using the Amaryllis Nucleics
252 YourSeq Duet Full Transcript library prep kit with combinatorial dual indexes (now Active Motif #23001
253 or #23002) according to manufacturer instructions. Prepared libraries were sequenced by Novogene with
254 Illumina NextSeq 500 (PE × 150bp). Arabidopsis RNA was also extracted using Qiagen's RNeasy kit,
255 per manufacturer's protocol. Total Arabidopsis RNA was sent to Novogene for mRNA-enrichment and
256 library preparation, then sequenced on Novogene's NovaSeq X Plus series (PE ×150bp).
257
258 ***GMUCT sequencing and RNA stability measurement***
259 GMUCT libraries were prepared as previously described (Willmann et al., 2014) using
260 approximately 10 μg of total RNA isolated from the same leaf tissue used for RNA-seq. GMUCT data
261 analyses was performed as previously described (Ganguly et al., 2025), and quality-controlled by
262 ensuring the presence of exon-junction complex footprints in our data. Both RNA-seq reads and GMUCT
263 reads were processed with Hisat2 for mapping and EdgeR to generate RPM-normalize counts (Kim et
264 al., 2019; Chen et al., 2025). mRNA degradation assay was performed as descried (Jia and Le, 2020).
265 Briefly, seven-day-old *Arabidopsis* seedlings of Col-0 and *dus2* were transferred from ½ MS solid medium
266 to ½ MS liquid medium in 12-well culture plates and incubated for 12 hours under 22 °C (control: 8 hours)
267 or 37 °C (heat treatment: 8 hours). Transcriptional inhibitor cordycepin (final concentration = 0.6 mM;
268 Sigma-Aldrich, C3394) was then added to each well for transcriptional arrest. Tissues (~10 seedlings per
269 biological replicate *3) were collected at 0 h, 15 min, 30 min, 1 h, 2 h, and 6 h after cordycepin treatment
270 for RNA extraction. After the same process of RNA-seq data using Hisat2 alignment and Feature Count
271 pipeline as mentioned above (Liao et al., 2013; Kim et al., 2019), normalization of decay assay was
272 followed as described (Sorenson et al., 2018). Briefly, read counts per gene were normalized based on
273 library size and scaled to 1 million [reads per million (RPM)], further scaled using 30 stable transcripts-
274 derived RNA decay factor to reflect the fact of decreasing total mRNA in the pool during transcriptional

275 arrest (https://rdrr.io/github/reedssorenson/RNAdecay/f/). Decay rate (K) and mRNA half-life were
276 calculated using exponential regression model $y(t)=Ae^{-kt}$, $t_{1/2}=\ln 2/k$ (A: T_0 normalized abundance, K:
277 decay rate, t1/2: half-life) and non-linear least square model $y(t)=Ae^{-k}t+C$, half-life: $t_{1/2}= -1/k*\ln(0.5-C)/A)$
278 (A: T_0 normalized abundance, K: decay rate, t1/2: half-life, C: residue) based on in house R scripts.
279

280 ***5'-6'-Dihydrouridine quantification***

281 Total RNA (1 µg) from *Arabidopsis* leaves was digested to nucleosides using Nuclease PI (0.6 U,
282 Sigma-Aldrich), phosphodiesterase I (0.2 U, Worthington), FastAP (2 U, Thermo Fisher), benzonase (10
283 U, Sigma-Aldrich), and pentostatin (200 ng, Fisher Scientific) in 25 mM ammonium acetate buffer (pH
284 7.5). Reactions were incubated overnight at 37 °C and stored at −80 C prior to LC–MS/MS. Digestion
285 enzymes were removed by 75% MeOH precipitation and centrifugation (21,000 g, 10 min); the
286 supernatant was dried and reconstituted in HPLC-grade water. LC–MS/MS was performed on a Waters
287 Acquity UPLC system coupled to a Xevo TQ-XS triple quadrupole mass spectrometer using an HSS-T3
288 Premier column (1.8 µm, 100 × 2.1 mm). Mobile phases were water + 0.1% formic acid (A) and
289 acetonitrile (B), run with a standard gradient at 0.3 mL min^{-1}. Dihydrouridine was monitored in positive
290 ESI mode (MRM, 247 → 114.9 m/z) with capillary voltage 1 kV, cone 40 V, and desolvation 400 °C.
291 Quantification was based on an external calibration curve using a 5,6-dihydrouridine standard (AdooQ
292 Bioscience).
293

294 ***Identification and characterization of DHU***

295 Identification of RCMs was performed by intersecting results derived from the High-throughput
296 Annotation of Modified Ribonucleotides (HAMR v1.4) and ModTect (v1.1.5.1) algorithms for sorghum
297 RNA-seq data (Vandivier et al., 2015; Tan et al., 2021). Initially, the paired-end stranded RNA reads were
298 trimmed by Trimmonmatic (v0.32, parameter: TruSeq3-PE.fa:2:30:10:2) to remove adaptors and low-
299 quality reads (Bolger et al., 2014). For HAMR, the forward and reverse reads were mapped to the
300 sorghum reference genome (v3.1.1) using Tophat2 (v2.1.1, --read-mismatches 12 --read-edit-dist 12, --
301 max-hits 10, --lib fr-second strand) (Kim et al., 2013; McCormick et al., 2018), followed by the merging of
302 mapped, removal of multiple-mapped reads, and resolving of splicing alignment using Picard (v3.1.1)
303 and GATK (v3.3.5, (McKenna et al., 2010). Detection were further processed by HAMR with a stringent
304 parameter setting: --min_read_qual 30, --min_read_coverage 50, --hypothesis H_4, --max_FDR 0.05,
305 which filtered out potential modified sites with a < 50 mapping depth with high-confidence (*FDR* < 0.05)
306 to call modified sites (Vandivier et al., 2015). For ModTect prediction, trimmed reads were mapped to the
307 sorghum genome and associated annotation files using STAR (v 2.7.10b(Dobin and Gingeras, 2015) with

308 the default arguments and ModTect with the following arguments: --minBaseQual 30, --readlength 150.
309 Only the overlapped sites derived from two replicates and two methods were retained as the modified
310 sites for each sorghum sample. The type of RCMs was further classified using a XGBoost-based machine
311 learning model (Palos et al., 2024). The output file of Modtech or HAMR was cross-referenced to the
312 gene annotation files to assign sites to transcripts. Here, the ratio of modified reads over total mapped
313 reads per transcript was calculate as RCM level. Location of DHU sites in sorghum and Arabidopsis
314 dataset were generated following workflow of MetaPlotR (https://github.com/olarerin/metaPlotR). The
315 ±1pb flanking regions of each DHU sites were harvested to calculate the portions of 3nt motifs around
316 DHU sites.
317

318 ***Population-level genomic analyses in sorghum***

319 Orthologs between Arabidopsis and sorghum were searched based on phytozome12 annotation and
320 confirmed using CoGeBlast (https://genomevolution.org/coge/CoGeBlast.pl, parameters E-value: 1e-5,
321 word_size: 3, matrix: BLOSUM62, TAIR 11 and Sbicolor_454.v3, (Cheng et al., 2017; McCormick et al.,
322 2018). The genomic variants of the six sorghum accessions were identified and annotated using sorghum
323 Association Panel (SAP) data (Boatwright et al., 2022). Briefly, trimmed DNA reads were mapped to the
324 sorghum reference genome (BWA-mem: v0.7.17-r1188, (Li, 2013). Duplicated read-pairs and low-quality
325 mapping in each sample were cleaned using Sambamba (Tarasov et al., 2015) (v1.28.1,
326 mapping_quality >= 1 and not (unmapped or secondary_alignment) and not ([XA] != null or [SA] != null).
327 Variant calling was conducted using the GATK4 HaplotypeCaller function (v4.2.5.00, parameters: --max-
328 alternate-allele:6, --Ploidy:2, (McKenna et al., 2010). The single nucleotide polymorphisms (SNPs) were
329 filtered using GATK hard-filtering (https://gatk.broadinstitute.org). Those high-quality variants were
330 further annotated by variants effect predictor (VEP) using the *S. bicolor* Sbicolor_454.v3 gene annotation
331 (McLaren et al., 2016). For phylogenetic analysis, we retained the bi-allelic SNPs at the four-fold
332 degenerate (4DTV) loci filtered by plink (v1.90b4, --types SNPs -m 2 -M 2) that derived from 365 out of
333 407 sorghum accessions with complete geographical information (Boatwright et al., 2022). Using the
334 SNP filtering with minor allele frequency (MAF > 0.05, missing data < 0.1) and linkage disequilibrium (LD)
335 prune (plink v1.90b4 parameter: --indep-pairwise 1000 500 0.2, (Purcell et al., 2007), a total of 7,520
336 SNPs were kept to reconstruct the phylogenetic tree using IQtree (v1.6.12, Parameter: -nt 100 -m MFP,
337 (Nguyen et al., 2015).
338

339 ***Transcriptome data processing***

340 All RNA-seq reads were trimmed using trimgalore (v0.6.10, -paired, -length 10) and mapped to
341 respective reference genomes using Hisat2 (v2.1.0, default setting, (Krueger, 2015; Kim et al., 2019).

342 FeatureCounts was used for reads quantification (v2.0.1, parameter: -s 1 -p -t mRNA -g ID -O) and further
343 normalized using DESeq2 after the removal of transcripts with less than an average of one count across
344 samples (Liao et al., 2013; Love et al., 2014). For sorghum, time point, accession IDs, and watering
345 conditions were incorporated as the experimental design factors. In Arabidopsis with Condition (Control
346 and Heat) and genotype (Col-0 and *dus2*) included for experimental design Condition-wise differentially
347 abundant transcripts (DATs) over each time point per accession were identified using the cutoff of false
348 discovery rate (*FDR* < 0.05). A $\log_2$-transformed fold change (FC) > 1 or < -1was used to filter up (down)-
349 regulated transcripts down-regulated transcripts. Z-score (row-based) normalization was performed to
350 visualize sample-wise heatmap. TPM (transcripts per kilobase million) were used for comparison of
351 transcript abundance across samples for all transcripts.
352

353 ***Proteomic data processing***

354 **Proteolytic Digestion:** Protein pellets were resuspended in 100 mM Tris-HCl buffer (pH 8.5) containing
355 4% (w/v) sodium deoxycholate. Proteins were reduced with 10 mM TCEP and alkylated with 40 mM
356 chloroacetamide, then incubated at 45 °C for 5 min with shaking (2000 rpm). Trypsin (in 50 mM
357 ammonium bicarbonate) was added at a 1:100 enzyme-to-protein ratio (w/w), and digestion was carried
358 out overnight at (37 °C with 1500 rpm). After digestion, SDC was removed by phase extraction. Samples
359 were acidified to 1% trifluoroacetic acid and desalted. Peptide concentrations were measured using the
360 Pierce Quantitative Colorimetric Peptide Assay Kit (#23275) following the manufacturer's instructions.
361 **LC-MS/MS for DIA Samples:** ~200ng sample was made onto a RSLC column and washed for 5 min
362 with buffer A (www.thermo.com). Bound peptides were then eluted over 35 min onto a RSLC resolving
363 column (gradient: 5%B to 38% B). After the gradient, the column was washed with 90% B for the duration
364 of the run (Buffer A = 99.9% H_2O, 0.1% formic acid, Buffer B = 80% Acetonitrile, 0.1% formic acid, 19.9%
365 H_2O, flow rate 400nl/min). Eluted peptides were sprayed into a Q-Exactive HF-X MS (www.thermo.com)
366 for data independent acquisition. Survey scans were taken in the Orbi trap (45000 resolution, determined
367 at m/z 200, mass range: 400-1000m/z. Fixed windows of 20m/z (34 total) with 1m/z overlapping margins
368 were sequentially scanned and fragmented by HCD acquired in the Orbitrap at 15,000 resolutions.
369 **DIA Data Analysis:** Acquired spectra were processed using DIA-NN (v1.8.1, (Demichev et al., 2020),
370 using the Robust LC (high precision) quantitation strategy with RT-dependent cross-referencing and
371 Deep Learning enabled in library-free mode against Arabidopsis protein sequences available from
372 Uniprot (www.uniprot.org) and search parameters were optimized by DIA-NN, and results filtered at a
373 precursor *FDR* of 1%.
374

375 ***Nanopore Direct RNA-sequencing (DRS)***

376 Poly(A) tailed RNA was extracted from Arabidopsis wild-type and *dus2* seedlings using 2-3 ug of
377 total cellular RNA or in vitro transcribed transcriptome RNA. Nanopore direct RNA-seq libraries were
378 generated and barcoded following the manufacturer's instructions (SQK-RNA004). Barcodes were
379 associated with read IDs using SeqTagger (Pryszcz et al., 2025). Raw files were base-called using
380 Dorado (v1.0.0: https://github.com/nanoporetech/dorado) with the following arguments: -v sup,
381 inosine_m6A_2OmeA, 2OmeG,m5C_2OmeC, pseU_2OmeU,--emit-moves, and --min-qscore 10. BAM
382 files were then demultiplexed by filtering for the relevant read IDs from SeqTagger using Samtools and
383 fastq file conversion (Li et al., 2009; Pryszcz et al., 2025). Fastq files were mapped to the *Arabidopsis*
384 transcriptome using Minimap2 (v2.29, parameter: -y, -ax map-ont, and -L (Li, 2018). Nanocompore
385 algorithm was utilized to detect *dus2* dependent modified sites (Leger et al., 2021). First, signal alignment
386 was performed using Uncalled4 (v4.1.0(Kovaka et al., 2021) with signal aligned BAM files used as input
387 to Nanocompore (depleted condition: *dus2*, min coverage: 10, chi-squared q-value < 0.05, GMM log odds
388 ratio > |0.3|).
389

390 ***Construction of co-expression networks***

391 The co-expression networks were constructed using the WGCNA package with variance stabilizing
392 transformed (VST) normalized read counts with 34,130 transcripts across 96 samples (Langfelder and
393 Horvath, 2008). Initially, a soft threshold (Beta score) was applied to fit the scale-free topology model
394 assumption which generates a minimum number to make the index curve flatten out reaching a high
395 value (>0.85) (Yu et al., 2024b). Further, the adjacency matrix represented by gene expression was
396 transformed into a topological overlap matrix (TOM) to classify genes using a dynamic tree-cut approach.
397 Finally, genes that shared high-confidence correlation (abs(coefficient) > 0.8) were merged into the same
398 module (parameter: deepsplit = 4, tree cut height = 0.2). The pairwise Pearson correlation between each
399 gene from modules and the module-wise eigengene values was tested to characterize each gene's
400 module membership (MM) under the same module. Lastly, the metabolite profiles, oxidative stress-
401 related enzyme activities, and LI-6800-derived traits were integrated into the network using Pearson
402 correlation between gene expression and these molecular phenotypes. Trait-correlated modules were
403 selected based on their correlation level between MM scores and phenotypes (cutoff: $r > 0.5$, or $r < -0.5$,
404 *p-value* < 0.05). The correlation between gene expression and phenotypes was estimated as gene
405 significance (GS) to interpret the importance of genes related to each molecular phenotype.

406 ***Functional and regulatory network analyses***

407 Functional enrichment analysis of pathways (Kyoto Encyclopedia of Genes and Genomes (KEGG)
408 database) and Gene Ontology (GO) analysis was performed to infer the biological function of genes

409 associated with certain RCMs, transcripts assigned in co-expression modules, and differentially abundant
410 transcripts. ShinyGO was used for GO and KEGG enrichment for both sorghum and Arabidopsis (*FDR*
411 < 0.05, (Ge et al., 2019). The protein-protein interactions (PPI) among genes present in the co-expression
412 network were acquired from the STRING database (parameter: confidence level: > 0.7, (von Mering et
413 al., 2003).
414

415 **Data visualization and usage of databases**

416 All statistical visualizations were generated in R (v4.3.2) with multiple packages. Briefly, plots include the
417 line, boxplot, PCA, and enrichment graphs generated by the ggplot2 package, and heatmaps using the
418 pheatmap package (Core Team, 2013). R Scripts used for plots were deposited in
419 (https://rpubs.com/LeonYu/Main-Figures and https://rpubs.com/LeonYu/Supp-Figures). The integrated
420 gene networks PPIs and co-expression derived from WGCNA were generated using Cytoscape
421 (Shannon et al., 2003).

422 # Results

423 ***Development of a diverse set of sorghum accessions with variation in their molecular and***
424 ***physiological responses to abiotic stress.***

425 Phenotypic diversity under drought conditions is ultimately traced to variation in genomic
426 sequence and rewiring of gene expression. Therefore, to capture the genetic and phenotypic diversity
427 present within sorghum, we initially generated a phylogeny from re-sequencing data for 356 out of 400
428 accessions with demographic information found within the sorghum association panel (SAP, (Boatwright
429 et al., 2022)**Figure 1A**). Cross-referencing this phylogeny with the SAP field trial (in Arizona in 2019)
430 under standard conditions, we selected six accessions to comprise a small but diverse panel based on
431 seed viability, genetic distinctiveness, and phenotypic variation (shoot and root biomass, plant height,
432 and yield). Among the selected lines, four accessions (A, B, E, and F) are African accessions, and the
433 other two accessions (C and D) are U.S. breeding accessions (**Figure 1A**). Variant calling and annotation
434 of variants were performed to examine the genomic variation between these accessions. In total,
435 8,725,449 variants were identified among the six accessions relative to the published reference genome,
436 with more than 50% of variants located in intergenic regions, followed by upstream and downstream gene
437 regulatory regions (21.0% and 19.5%, respectively), intronic regions (5.61%), and splicing regions
438 (0.23%; **Figure S1, left panel**). Approximately 10-20% of the genomic variation in the panel was
439 comprised of unique SNPs and INDELs specific to each genotype (**Figure S1 right panel**). In summary,
440 these data suggest that we were successful in selecting six distinct accessions, representative of the
441 genetic diversity within the species, and likely the wide range of environments in which sorghum can
442 grow.

443 To assess the performance of this panel under heat and drought conditions, we grew the six
444 accessions in replicated plots as part of a large field trial conducted during the summer of 2020. All plants
445 were well-watered (WW) until beginning of the reproductive stage (appearance of the flag leaf; 47 days
446 after planting; **Figure 1B**), after which irrigation was reduced for a subset of plots to mimic drought
447 treatment. Phenotypic measurements and molecular sampling (for transcriptomic, metabolomic, and
448 biochemical traits) occurred during the 1_{st}, 3_{rd}, 5_{th}, and 7_{th} week after the beginning of the drought
449 treatment (**Figure 1B**)**,** with destructive measurements (e.g., biomass and root microbiome composition)
450 occurring at the end of the season. Treatment effects were readily apparent at the end of the season
451 (**Figures 1C**), with the M1 ("A") accession showing the most pronounced leaf necrosis. Leaf level
452 physiological traits, such as water use efficiency (WUE) and CO_2 net assimilation (A_{net}) exhibited similar
453 results, with the "A" accession displaying hallmarks of water stress, particularly at the later time points
454 (week 5 and week 7, **Figure 1D**), whereas other accessions, such as "B" and "C", showed a more robust

response. Thus, in addition to genotypic diversity, these data suggest that these six accessions displayed phenotypic diversity to drought stress and may provide information on the molecular mechanisms by which sorghum responds to water limiting conditions.

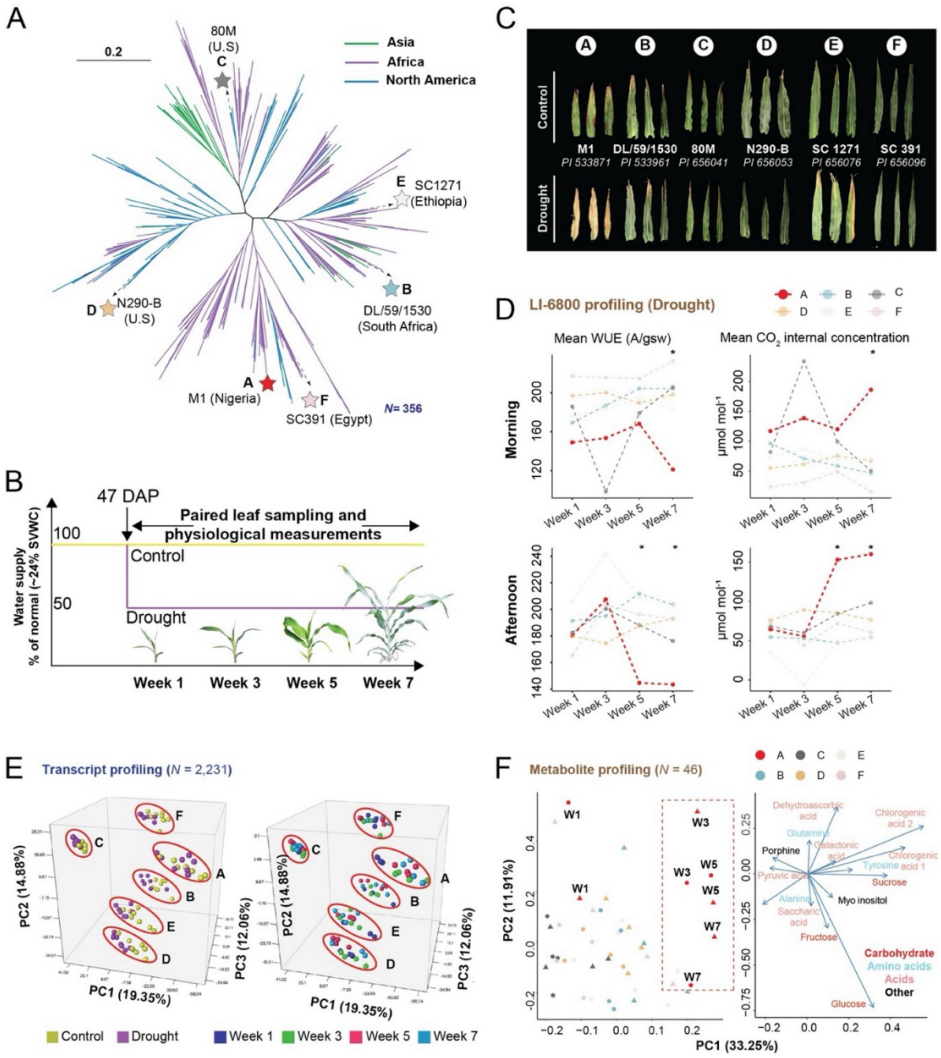

Figure 1. Drought tolerance diversity of selected sorghum genotypes
(A) Reconstruction of an unrooted phylogeny of the Sorghum Association Panel (SAP). The six sorghum accessions used in this study are marked along with the geographical locations colored to represent African (green), Asian(purple), and North American (blue) regions. The placement of the six accessions used in this study is denoted with different colored stars that match the color scheme throughout this work. (**B)** Six sorghum accessions were grown at the Arizona in the field with treatment (reduced water supply) imposed 47 days after planting (DAP). Paired molecular sampling (RNA-seq, metabolites, and oxidative stress chemicals), were collected alongside physiological measurements (e.g., LI-6800 photosynthesis-related traits). **(C)** Representative leaf tissue collected at the terminal stage of sampling in the field is shown. **(D)** Line graphs denote the mean WUEi and internal CO_2 concentration values measured during the morning (top) and afternoon (bottom) at each time point for drought-treated plants (N = 5 per accession). Asterisks indicate significant differences of parameters derived from the comparison of each accession relative to "A" ($p < 0.05$). **(E)** Two principal component analyses (PCAs), based on the top 10% most abundant transcripts, highlight the separation caused by genotypic and treatment effects (left) and genotypic and temporal effects (right). **(F)** The left PCA displays separation based on treatment (triangle = drought; circle = control) and genotype (colors similar to those in panel C). The right PCA loading plot highlights major contributors to the left PCA, with the length of the line denoting the contribution of a particular molecule to the PCA.

476 ***Sorghum accessions display variable molecular responses to stress***

477 To characterize the molecular responses to water limiting conditions in our panel, we next
478 assessed the change in transcript abundance over the two months of the treatment (Weeks 1, 3, 5, and
479 7) using RNA-seq. Initial quality control revealed high correlation between replicates (Pearson Correlation;
480 r > 0.95, **Table S1**). To unpack the transcriptomic responses to treatment in the six accessions, we
481 examined the top 10% of most variable transcripts based on the standard deviation (SD) of the global
482 transcript abundance for principal component analysis (PCA). This approach uncovered strong genotypic
483 and treatment effects represented by both PC1 and PC2, with accession "C" exhibiting the least
484 separation due to stress or time, and accession "A" exhibiting the most (PC1 = 19.35%, PC2 = 14.88%,
485 **Figure 1E**).

486 To gather additional clues as to how these accessions responded to drought treatment at the
487 molecular level, we next examined the stress-induced changes in metabolites and oxidative stress
488 markers in sorghum leaves (Das and Roychoudhury, 2014; Obata et al., 2015). Metabolites and oxidative
489 stress markers were measured on leaf samples collected simultaneously with those used for RNA-seq
490 analyses, with GC-MS-based quantification and annotation of primary metabolites and
491 spectrophotometric-based quantification of oxidative stress markers. A PCA of global changes in the leaf
492 primary metabolome (*N* = 46) across our panel revealed that, as for the transcriptome, genotype
493 explained much of the variation between samples (**Figure 1F**, left panel; PC1: 33.25 %). Interestingly,
494 samples associated with accession "A", weeks 3, 5, and 7 (both conditions), separated from all other
495 samples, and this separation was largely driven by levels of the three main soluble sugars (sucrose,
496 glucose and fructose) and chlorogenic acid (**Figure 1F**, right panel). Overall, we identified strong
497 genotypic effects for both visible and molecular phenotypes. As expected for this species, most
498 accessions displayed resilience under stressed conditions, whereas accession "A" performed poorly in
499 under stress conditions. Thus, this panel presents a suitable comparative framework to examine
500 transcriptional and post-transcriptional regulators of drought and heat stress responses in sorghum under
501 field conditions.

502

503 ***Integrated network analysis uncovers a link between DHU and photosynthesis traits***

504 With each of these molecular and physiological traits examined, we next took a comparative
505 systems-level approach to connect these traits to their molecular pathways and putative regulators. To
506 do so, we constructed a co-expression network starting with the top 10% of most variable transcripts, as
507 measured by median absolute deviation (MAD) score. We then recursively increased the number of
508 included transcripts until we achieved an optimized network with the fewest number of unassigned
509 transcripts and the highest scale-free topology model (**Table S2**). The resulting network contained 22,314

510 transcripts classified into 29 modules with a low proportion of unclassified transcripts (*N* = 2,982) and
511 high scale-free model correlation (*r* = 0.91, slope = -1.93, **Table S2**). Using this framework, we
512 incorporated phenotypic data into modules using trait-module correlation. Briefly, the first principal
513 component value (eigenvalue) per module was calculated using their transcript abundance PCA. Leaf-
514 level physiological measurements (LI-6800), metabolite abundances, and oxidative stress marker
515 abundances were then correlated with the eigenvalues of each module (**Table S3**), leading to 19 modules
516 with significant trait-module correlations ($p < 0.05$, **Figure 2A**, left panel). Several modules (e.g. "blue",
517 "greenyellow", "pink", and "purple") were strongly correlated with multiple traits. For instance, "blue",
518 "purple", and "pink" modules are closely related to most photosynthesis traits (> 90% LI-6800 entries),
519 whereas "purple" and "greenyellow" modules are highly correlated with many metabolic traits and
520 oxidative stress chemical abundances (**Figure 2A**).

521 To gain insights into the biological processes associated with modules, module-wise GO and
522 KEGG enrichment analyses were performed (modules with *FDR* < 0.05 are displayed, **Figure 2A**, top
523 panel). This approach revealed modules with biological processes of interest, such as stress response
524 ("blue", "red", and "pink"), RNA processing and modification pathways ("blue", "greenyellow", "purple",
525 "midnightblue", and "lightyellow"), and photosynthesis terms ("blue", **Figure 2A and Table S4**).
526 Specifically, in addition to the observed module-trait correlation, the "blue" module was strongly enriched
527 for transcripts associated with photosynthesis traits (eg: net CO_2 assimilation: r = 0.72) based on both
528 GO and KEGG terms (fold change > 5, *FDR* < 0.05, **Table S4**). Interestingly, an examination of eigengene
529 values within this module revealed a strong genotypic effect, where transcripts derived from the "A"
530 accession cluster separately from the other accessions (**Figure 2B**), and therefore may explain the
531 physiological distinctiveness of this accession. Given the strong trait module correlations and the over-
532 representation of stress and photosynthesis associated genes, the "blue" module thus represents a
533 strong link between phenotypic and molecular responses to stress treatment.

534 A close examination of genes with strong module membership (kME; **Table S5**) in the "blue"
535 module revealed two genes encoding putative dihydrouridine synthases (DUS), which convert uridine to
536 dihydrouridine (DHU; Sobic.006G158100 and Sobic.006G038500). A phylogenetic analysis using a
537 maximum likelihood tree derived from an amino acid sequence alignment of human, fission yeast,
538 budding yeast, and multiple plant DUS proteins suggests that Sobic.006G158100 is more similar to
539 eukaryotic DUS2 (**Figure S2**; SbDUS2), whereas Sobic.006G038500 fell into the DUS3 clade (**Figure**
540 **S2**; SbDUS3). A third sorghum DUS, Sobic.010G262000, fell into the DUS1 clade but was not found to
541 be associated with plant performance traits within the "blue" module (SbDUS1). The strong association
542 between these two genes and the blue module implies that their transcriptional regulation, and potentially
543 their function, is associated with plant performance under stress.

544 Given the inclusion of DHU synthase in the stress and photosynthesis-related "blue" module, we
545 examined the RNA-seq data for hallmarks of RCMs that impact the Watson-Crick-Franklin base-pairing
546 edge. DHU belongs to a subset of RCMs that interfere with RNA-seq library preparation (specifically the
547 reverse transcription step), leaving patterns of mis-incorporated nucleotides that can be assigned to
548 specific modification classes bioinformatically (Vandivier et al., 2015; Helm and Motorin, 2017; Tan et al.,
549 2021). We thus processed our RNA-seq data through two independent RCM predictors (HAMR and
550 Modtect) and took the intersection of called sites (**Table S6**), resulting in 20,096 high-confidence RCMs
551 associated with 3,715 transcripts among the six main classes of HAMR/Modtect identifiable RCMs (**Table**
552 **S7**). Of these, a total of 3,008 DHU sites on 1,370 transcripts were detected, with 326 transcripts
553 associated with predicted DHU modification residing within the "blue" module (**Table S8**). To determine
554 if DHU is preferentially associated with photosynthesis and stress related transcripts in this module, we
555 performed KEGG enrichment of these 326 transcripts and a similar number of non DHU-modified (NDM)
556 transcripts within the module as background (random selection bootstrap = 10). This approach uncovered
557 an elevated enrichment level of "photosynthesis" terms in the DHU-modified sets compared with the "non
558 DHU modified" set (*FDR* < 0.05, **Figure 2C**). Lastly, to determine if there was a relationship between
559 DHU abundance and field-derived traits, a pair-wise Pearson correlation was performed between
560 transcript abundance and photosynthetic trait measurements (A, Ci, and gsw, respectively) for all DHU-
561 modified and a similar number of randomly selected non-DHU modified transcripts (**Figure 2D**). This
562 analysis revealed a strong correlation between transcripts associated with DHU modification and
563 photosynthetic traits, suggesting a close relationship between DHU modification status, transcript
564 abundance, and photosynthetic processes in sorghum.

565 We next assessed whether the transcriptomic accession-associated variation was also observed
566 in the DHU deposition on these 326 modified transcripts. A PCA revealed that the DHU status for these
567 transcripts in the "A" accession was markedly different at most time points and conditions relative to the
568 other accessions (PC1 was primarily explained by DHU variation in the "A" accession; **Figure 2E**). We
569 explored this accession-driven variation further by determining if the pattern of DHU deposition on these
570 transcripts was different in the "A" accession relative to the others. Based on a metaplot profiling of DHU
571 deposition on the 326 DHU-modified transcripts, we observed variation at both the 5' and 3' ends, with
572 the most dramatic variation near the 3' end of the CDS in the "A" accession relative to the others (**Figure**
573 **3F**). In sum, these data highlight the association between DHU status and photosynthesis, suggesting
574 that variation in this molecular phenomenon between accessions be linked to plant performance.

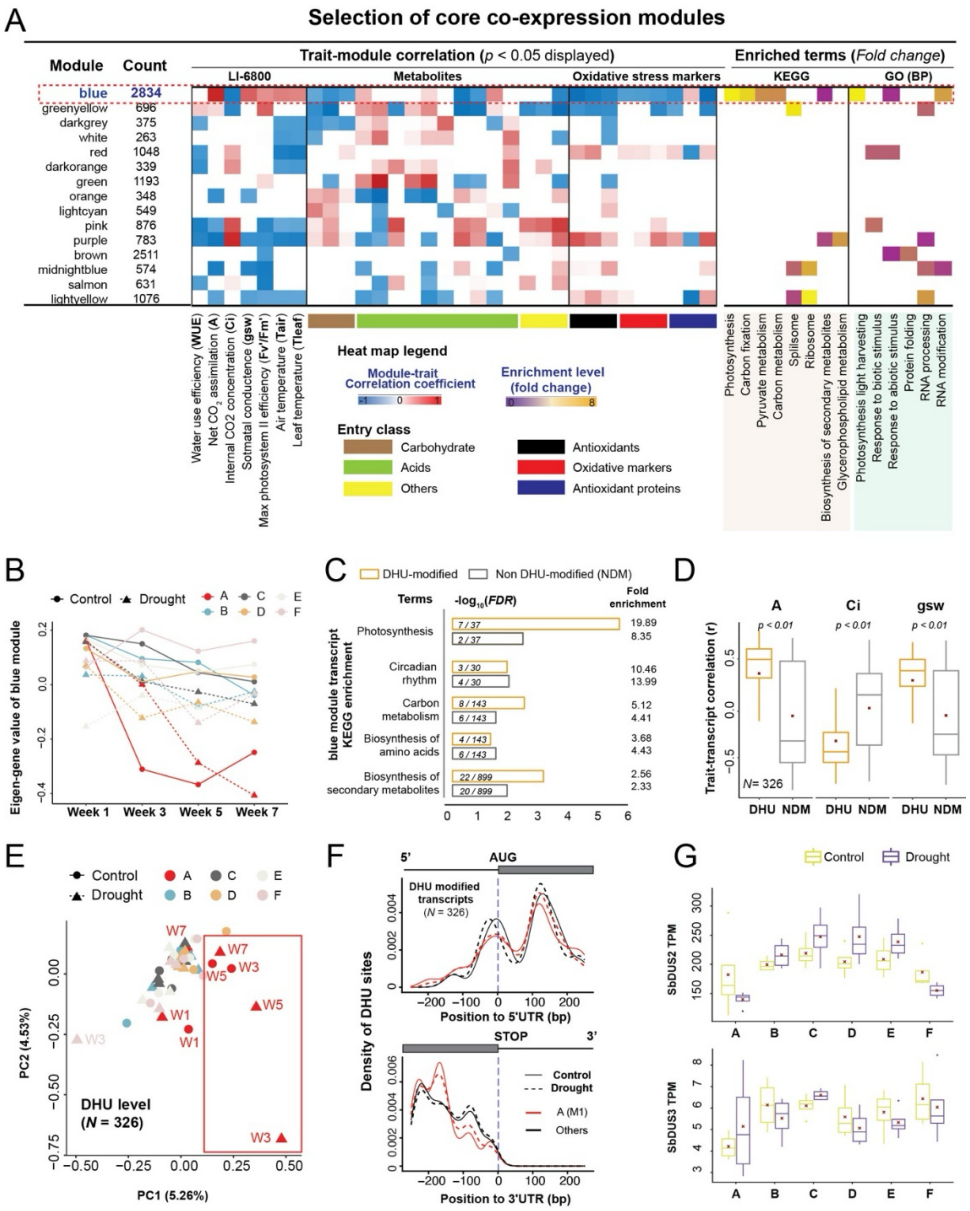

Figure 2. Selection of co-expression modules contributing to sorghum drought tolerance
(A) The number of transcripts per module, correlation between traits and the module (blue and red scale), levels of KEGG and GO enrichment levels (purple and brown scale), and the known proteins related to RCM recognition, deposition, and removal located in each co-expression module. Scales for module-trait correlation values (blue to red scale: -1 to 1), as well as GO-enrichment levels (purple to yellow scale: fold changes) are shown to the bottom left. Only those module-trait correlations and enrichment levels with a $p < 0.05$ are shown. **(B)** The eigenvalue of the photosynthetic module, divided by accession, treatment, and time, was plotted. (**C)** Correlation of transcript abundance and modification was compared between 326 transcripts been modified by both DHU and other RCMs in the blue module. **(D)** Bar plots denote the $\log_2(FDR)$ score of consensus enrichment terms, with number of genes associated with the term over the total genes in the term (middle), and the fold change for each term (right) **(E):** Box plots denote the correlation coefficient (r) between transcript abundance and each photosynthetic trait (A, Ci, and gsw) between DHU-modified group and the non-modified group. **(E)** Principal component analysis (PCA) of DHU-modified transcripts from the "blue" module (N = 326 transcripts). **(F)** Metaplot shows density of DHU sites across upstream (downstream) 250bp genomic region near start (stop) codon over 325 transcripts in accession "A" and other five accessions under control and drought conditions. (**G)** TPM of *SbDUS2* and *SbDUS3* across the two conditions and six accessions.

592 ***SbDUS2 is associated with DHU deposition on photosynthesis-related transcripts in***
593 ***sorghum under abiotic stress***

594 Because both SbDUS2 and SbDUS3 appeared in this DHU-associated module, we examined the
595 reproducibility of transcriptomic interactions within the "blue" module to help guide the selection of a
596 candidate for subsequent studies. To do so, we first developed a child network of all transcripts in the
597 "blue" module that shared high confidence edges with *SbDUS2* and *SbDUS3* and were DHU modified (*N*
598 = 29**, Figure S3A and Table S5**) and examined the relationship of these transcripts with both *SbDUS2*
599 and *SbDUS3* transcripts and DHU abundance. Interestingly, we observed a negative correlation between
600 DHU status and the abundance of these 29 interacting transcripts in our field data (**Figure S3B**). We then
601 examined the abundance of each of these transcripts in a publicly available sorghum tissue atlas dataset
602 (accession: BT×623; (McCormick et al., 2018). Not only where these 29 DHU-modified transcripts most
603 highly abundant at similar developmental stages in the sorghum tissue atlas as in our dataset, we also
604 observed a strong negative correlation between DHU levels and 11 out of the 29 focal transcripts (p <
605 0.05; **Figure S3C**). Notably, *SbDUS2* and *SbDUS3* were also predominantly expressed in leaf tissues,
606 and largely during late vegetative and flowering developmental stages, similar to our observations in our
607 six accessions (**Figure S3D**). We then asked which SbDUS most likely influences DHU deposition on
608 mRNAs within the "blue" module by assessing the correlation between the score of the first principal
609 component (PC1) of 326 transcripts-derived DHU PCA **(Figure 2E)** and the transcript abundance of
610 *SbDUS2* and *SbDUS3* (**Figure S3E).** This analysis revealed a stronger correlation between *SbDUS2*
611 and PC1 scores (r = -0.63, p = 1.4e-06) than for *SbDUS3 (r* = -0.39, p = 0.0064*)*, implying that SbDUS2
612 might be more tightly associated with DHU status. Additionally, *SbDUS2* exhibited significantly higher
613 transcript abundance (TPM) in both datasets (p < 0.0001, **Figure S3D and Figure 2G**). Not only was
614 *SbDUS2* on average ~40x more abundant than *SbDUS3* across the six accessions and in the sorghum
615 tissue atlas data, Sb*DUS2* also displayed an overall decreased transcript abundance under water limiting
616 conditions in the "A" and "F" accessions and an increase in all other accessions (**Figure 2G**), whereas
617 *SbDUS3* displayed no significant treatment effect. We also assessed *SbDUS1*, which was more highly
618 abundant than *SbDUS3*, but did not associate with transcripts in the "blue" module or performance-
619 related traits and displayed minimal transcript-level differences in response to treatment (**Figure S3F**).
620 Thus, based on its consistently high transcript abundance across two datasets and its stress-response
621 pattern, we focused analysis on DUS2 and its potential contribution to DHU modification under abiotic
622 stress conditions.
623

624 ***DUS2 mutants display DHU level reduction associated with growth and developmental***
625 ***delays in Arabidopsis***

626 Convinced that DHU was somehow linked to photosynthetic traits in sorghum, and that SbDUS2
627 was the likely enzyme responsible for DHU deposition on photosynthesis-associated transcripts, we next
628 turned to the genetic model, *Arabidopsis thaliana*, to gain a better understanding of how DHU might
629 impact plant performance. Based on our phylogenetic assessment of the DUS1/2/3 protein family across
630 eukaryotes, we identified the Arabidopsis *Dus2* ortholog, which encodes a protein that is 79.81% identical
631 to SbDUS2 at the amino acid level (**Figures S2 and 3A**). We obtained two T-DNA insertion lines that
632 disrupted the third and fourth exons, respectively, within the coding region of *AtDus2* (AT3G49640,
633 **Figure 3A**, CS857388 and SALK_079129C, https://abrc.osu.edu/). We confirmed that these insertions
634 disrupted *AtDUS2* transcription using both Illumina and Oxford direct RNA-seq (ONT-DRS; **Figure S4A**).
635 Loss of *AtDus2* resulted in a significant reduction of DHU based on LC-MS/MS of total RNA extracted
636 from mature rosette leaves (**Figure 3B; left, Table S9**), as well as a significantly lower global
637 HAMR/Modtect-derived DHU level not observed for other RCMs detectable by these algorithms (**Figure**
638 **3B; middle,** N = 8). Although a DHU-aware base-calling algorithm is not currently available for ONT-
639 DRS, as another layer of cross-validation, we used ONT-DRS to detect differentially "modified" U sites
640 between Col-0 and the *dus2* background that were not associated with the two currently detectable Uracil
641 modifications, Ψ or 2'-O-Me-U (**Figure 3B; right**). After excluding these modifications, we observed an
642 increase in modified U sites in Col-0 relative to the *dus2* background, suggesting that these modified
643 sites are AtDUS2 dependent. Based on HAMR/Modtect-derived data in both Arabidopsis (Col-0) and
644 sorghum samples, we observed DHU being deposited in a similar U-tract sequence context within
645 mRNAs as was observed in yeast (**Figure S5A**), with a preference for the CDS over UTRs (**Figure S5B**,
646 Finet et al., 2022b). These data suggest that DHU is found within Arabidopsis mRNAs, and that at least
647 a subset of them are dependent on *AtDUS2*.

648 In addition to diminished DHU levels, Arabidopsis *dus2* mutants displayed reduced germination
649 (**Figure 3C**; $p < 0.05$, $N > 50$) and slower growth rates, as well as shorter stature and increased time to
650 flower in both *Atdus2* mutant lines relative to wild-type controls (Col-0, **Figure 3D and Figure S4C and**
651 **S4E**), although the *Atdus2* mutants eventually reach normal height relative to Col-0 (**Figure S4F**).
652 Ultimately, these phenotypes led to an extended period of vegetative growth and delayed leaf
653 senescence in *Atdus2* relative to Col-0 (**Figure 3D**), confirming that loss of AtDUS2 leads to abnormal
654 growth and development under control conditions.

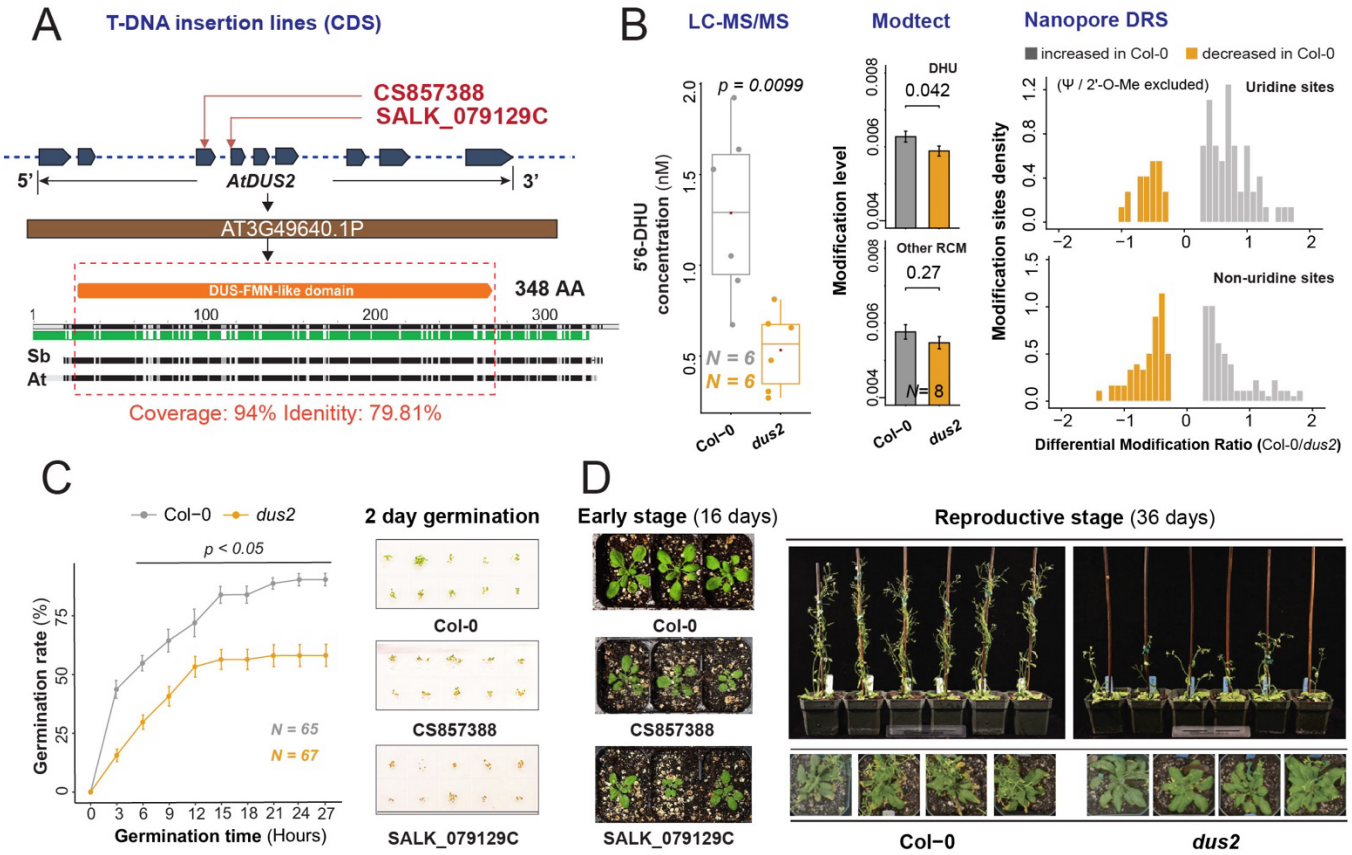

Figure 3. Characterization of the *dus2* mutant in Arabidopsis
(A) Schematic of the *AtDUS2* locus (top) with the T-DNA insertion sites in the third and fourth exon denoted. A protein alignment of the Arabidopsis and sorghum DUS2 proteins is depicted below, with the DUS-FMN-like domain outlined in orange. Alignment coverage and amino acid identity is shown below. **(B)** Left: Comparison of 5,6-dihydrouridine between two genetic backgrounds using LC–MS/MS analysis of hydrolyzed total RNA with external calibration using synthetic 5,6-dihydrouridine standards under (10, 50, 100 nM); Middle: Density plot of significantly modified sites (q-value < 0.05) between Col-0 and *dus2* of uridine-associated/non-uridine associated sites using Nanopore DRS**. (C)** Quantification based on imaging of seeds grown on MS plates, with each datapoint representing three plates. Germination was calculated as the full emergence of cotyledons with images after 2-day germination **(D)** Top-view images of two independent dus2 T-DNA insertion lines at 2-week of growth (left). Side images of the two backgrounds at the point of silique maturation for Col-0 (36 days; top), and top-view images of the rosettes captured at the same timepoint (bottom).

Given the importance of DHU for function of other classes of RNAs, we next assessed whether the *Atdus2* mutant background exhibited an mRNA and protein-level response that might explain the observed delayed growth phenotype. To explore transcriptomic and proteomic responses, we compared profiles from mature rosette leaves of *Atdus2* mutants versus Col-0 controls. Illumina RNA-seq was used to determine which transcripts were differentially abundant and untargeted LC-MS/MS was used to determine if protein abundance was impaired by loss of *AtDus2*. Loss of *AtDus2* led to 807 and 1,096 transcripts with increased and decreased abundance, respectively (*FDR* < 0.05, $|\log_2 FC| > 1$; **Figure S6A, Table S10**). At the protein level, 2,901 proteins with reproducible detection across replicates (*N* = 3 per genotype) were examined for changes in abundance between *Atdus2* and Col-0. We found 128

678 and 147 proteins with increased or decreased abundance (*padj* < 0.05; **Figure S6B**), respectively, in the
679 mutant, with a strong positive correlation in the change between genotypes between transcript and
680 protein abundance observed for those where matching data were available (N = 275, r = 0.43 and p =
681 1.7e-13, **Figure S6C**). We then integrated the status of RNA, DHU, and protein abundance in the two
682 genetic backgrounds, focusing on a set of 38 DHU modified transcripts that displayed differential
683 abundance at all three levels between Col-0 and *Atdus2* backgrounds (**Table S11**). This subset displayed
684 a strong positive correlation between transcript and protein abundance (r = 0.54, p = 0.00047; **Figure**
685 **S6D**), and a negative correlation between DHU levels and protein abundance (r = -0.35, p = 0.038; **Figure**
686 **S6E**). These data suggest that DHU is predominantly, but not always, negatively associated with mRNA
687 and protein abundance.
688

689 ***AtDus2 loss-of-function leads to alterations in mRNA stability***

690 Given the observed negative relationship between DHU level and mRNA abundance in both
691 Arabidopsis and Sorghum, we next assessed whether DHU was impacting RNA stability. We first
692 examined differences in global uncapped mRNA profiles between Col-0 and *Atdus2* using the genome-
693 wide uncapped and cleaved transcripts (GMUCT) approach (Gregory et al., 2008; Willmann et al., 2014).
694 In this framework, a higher proportion of uncapped transcripts (GMUCT reads/ RNA-seq reads) indicates
695 reduced mRNA stability, whereas a lower proportion suggests enhanced RNA stability. To assess data
696 quality, we ensured the captured of exon-junction complex footprints in our libraries for both genotypes
697 (Lee et al., 2020). Using HAMR/Modtect detection, we identified a total of 426 DHU-modified transcripts
698 in Col-0 under control condition, and 302 of these transcripts were associated with reduced DHU levels
699 in the *Atdus2* background (**Table S12**), suggesting their DHU status was *AtDUS2* dependent. These
700 DHU-level dependent transcripts were not only more abundant at transcript level in the *Atdus2*
701 background relative to non DHU-modified transcripts based on cumulative frequency (**Figure S7A,** p <
702 1e-16, solid lines), GMUCT also uncovered a significant reduction in the proportion of uncapped RNAs
703 in the *Atdus2* background relative to Col-0 (**Figure 4A**, blue boxplots, p = 0.00087). This reduction was
704 not observed for non DHU-modified transcripts (**Figure 4A**, red boxplots, p = 0.25), suggesting that the
705 presence of DHU on these transcripts in a Col-0 background was influencing their degradation.

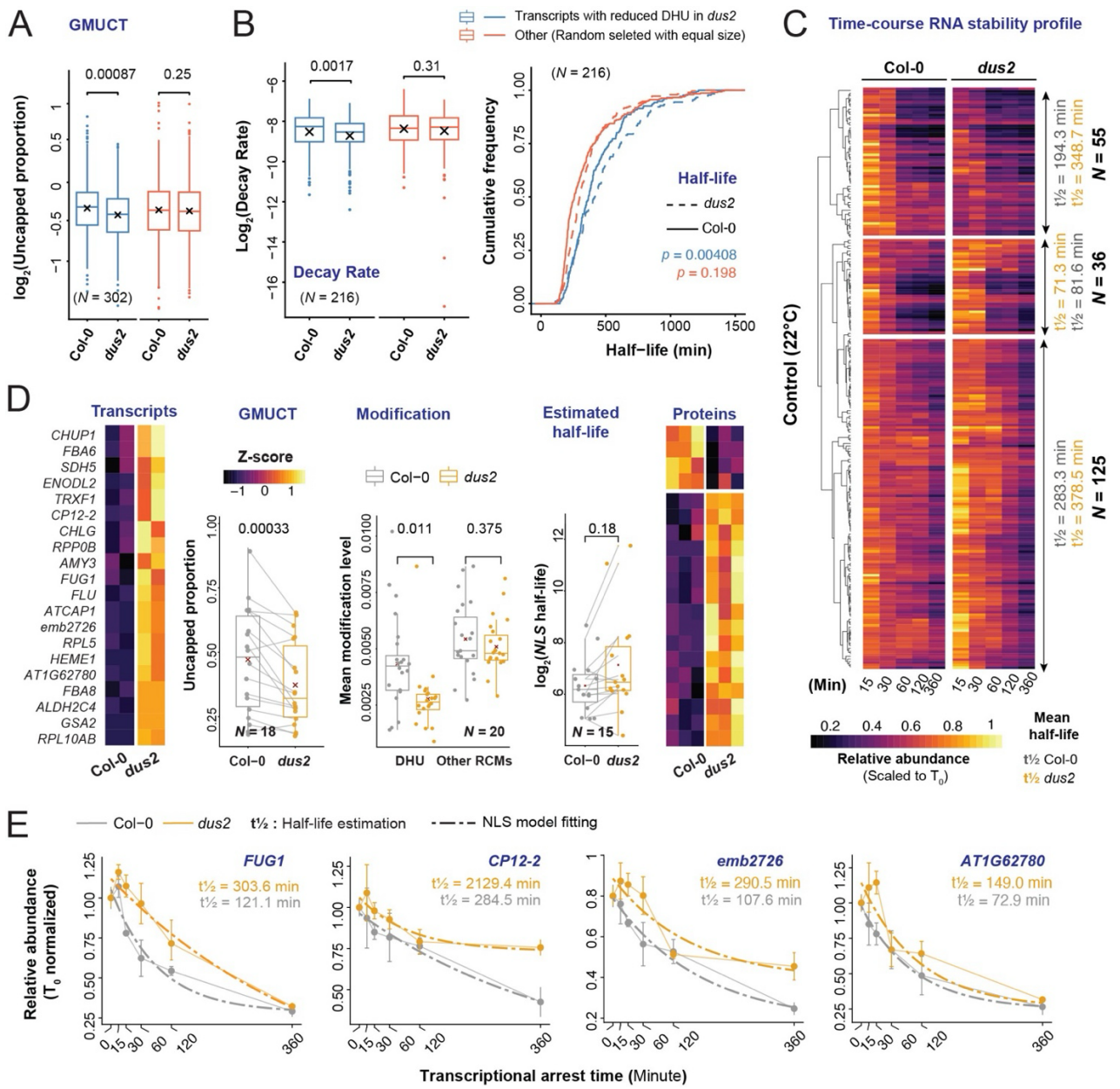

Figure 4. Altered RNA stability between Col-0 and *dus2* background

(A) Boxplot shows comparison of GMUCT-derived uncapped portions per transcripts over transcripts associated with lower DHU level in *dus2* (blue boxplots) and other transcripts (red boxplots) in Col-0 and *dus2* background, examinate by Wilcox test. **(B)** Decay rate (*K*) on groups of transcripts with lower DHU level in *dus2* mutants (blue boxplots) were compared with subset of randomly selected transcripts with equal sample size (red boxplots) using t-test ($p < 0.05$) on the left; Cumulative frequency of estimated half-life of transcripts in Col-0 (solid line) and *dus2* (dashed line) background with lower DHU level in *dus2* mutants (blue lines) were compared with randomly selected transcripts (red lines) on the right. **(C)** Heatmaps show differentiated decay rate of transcripts derived from panel (B), which majority faster decay in Col-0, partial similar decay between two genotypes, and small groups with slower decay in Col-0 under both control and heat conditions. **(D)** Heatmap of 20 transcripts associated with differential DHU, transits abundance, and protein abundance was plotted. Boxplots show GMUCT and RNA modification level of 16 transcripts with reduced protein in Col-0 relative to *dus2* (Wilcox test, $p < 0.05$), along with estimated half-life comparison of14/16 transcripts (Wilcox test). **(E)** RNA decay curve 6-hour experiment and line graph (error bars displayed) of four selected transcripts associated with higher DHU level and faster degradation in Col-0 than *dus2*, with estimated half-life were using NLS model.

722 To further test this model, we performed a time course transcriptional arrest experiment, treating
723 7 day-old Arabidopsis seedlings with the transcription inhibitor, cordycepin over a period of six hours
724 (**Figure S7B**). After QC (correlation among replicates > 0.9, aligmnet rate > 90%) and data normalization
725 based on (Sorenson et al., 2018), including the removal of low-abundance transcripts at T_0 and transcripts
726 with high standard error (T_0 average TPM > 8 and SE < 0.5), we retained 12,450 trancripts for modeling
727 using both an exponential regression model (*Exp*) and a nonlinear least squared model (NLS) to estimate
728 the decay rate (*K*) and half-life (min) for each transcript (**Supplementary Table 13**). Using either model,
729 we did not observe a significant change in global RNA decay rates (**Supplementary Table 13**). However,
730 when examining just those transcripts for which we could assign DHU status and model decay rates
731 (216/302 transcripts with reduced DHU in *dus2*), we saw both a significant decrease in decay rates and
732 corresponding increase in mRNA halflives (**Figure 4B;** left = decay rate, right = half life estimation). These
733 216 DHU-modified transcripts could be further divided into three groups based on their half-life patterns
734 using clustering as a reference (**Figure 4C and Figure S8A,** average half-lives denoted for each cluster),
735 with a great portion all displaying a longer half-life in the *Atdus2* background (*N* = 125; **Figure 4C**).
736 Interestingly, these more stable transcripts were predominantly associated with photosynthetic and
737 translation-related GO-terms (**Figure S8B, top**). These data suggest that, in agreement with the GMUCT
738 data, DHU is predominantly marking unstable or degrading transcripts.
739 We next returned to the 38 transcripts for which we saw links between DHU, transcript, and protein
740 abundance (**Figure S6D and S6E**). Of these, 20 showed both increased transcription and significantly
741 reduced DHU levels in the *Atdus2* background (p = 0.011; **Figure 4D middle**) with 16 out of these 20
742 displaying significantly increased protein abundance. As expected, these transcripts displayed limited
743 variation in non-DHU RCMs detected by HAMR/Modtect (p = 0.375). These differentially DHU-modified
744 transcripts are involved in KEGG-defined metabolic pathways, ribosome function, and photosynthesis-
745 related processes, with most (14/20) localized to either the chloroplast or mitochondria, although these
746 transcripts originate from the nuclear genome (**Table S11**). A majority of these DHU modified transcripts
747 with sufficient GMUCT coverage (15/18) also displayed a significant decrease in the proportion of
748 uncapped reads relative to Col-0 (p= 0.00033, **Figure 4D middle**), suggesting DHU-dependent transcript
749 degradation. Half-life modeling largely agreed with this model of DHU-dependent degradation, as 12/15
750 transcripts (with sufficient data to model) showed an increased half-life in the *Atdus2* background, with
751 half-life estimates increasing by ~2-10 fold for four transcripts as displayed (**Figures 4E**, full dataset and
752 modeled rates found in **Supplementary Table 13**). Thus, under normal growth conditions, DUS2, and
753 the RCM DHU, appear to be important for turnover of a core subset of transcripts associated with
754 photosynthesis and metabolism.
755

DHU impacts photosynthesis-associated traits under abiotic stress in Arabidopsis

Given SbDUS2's connection to performance under abiotic stress in sorghum, we next sought to validate this role in the context of a *Atdus2* loss-of-function background in Arabidopsis plants. First, we assessed whether there was a DUS2-dependent impact on plant performance under the two main stressors sorghum experienced in the field, water deficit and heat stress, applied separately here for Arabidopsis. We monitored vegetative growth and development of Col-0 and *Atdus2* mutants seedling (SALK_079129C and CS857388) under water withholding or heat stress conditions. Water withholding was performed by reducing soil water content (SWC) from 70% (control conditions) down to 25% (drought) over six days and then holding SWC at 25% for three additional days on four-week-old seedlings, with images been analyzed to estimate approximate growth rates (**Figures 5A and S4B**). As expected, Col-0 plants displayed reduced rosette area under water withholding conditions, indicating that the stress was successfully applied to these plants (**Figure 5B**). Plants lacking *Atdus2* showed a significant ~50% reduction in rosette area relative to Col-0 under both control and water withholding conditions (**Figures 5B** and **S4C**). Heat stress, applied to two-week old seedlings for 12 days, resulted in a similar relative decrease in plant growth for both Col-0 and *Atdus2* mutants, however, the *Atdus2* mutant backgrounds showed significantly reduced survival rate at the end of the experiment (**Figures 5C** and **5D**). Seven-day-old *Atdus2* mutant seedlings showed a similar response when exposed to heat stress for 72 hours (37ºC) on ½ MS plates, suggesting this is a robust sensitivity to heat stress. We next assessed photosynthetic capacity via the LI-6800 system (net CO_2 assimilation) in both the Col-0 and *Atdus2* drought and heat stressed plants (**Figure 5E**). Interestingly, we observed a slight, but non-significant decrease in net CO2 assimilation under control conditions between *Atdus2* and Col-0, whereas the *Atdus2* background showed a significant reduction under both stress conditions (p <<< 0.05 in both treatments; **Figure 5E**). These data suggest that AtDUS2, and DHU, is important for full photosynthetic capacity under drought and heat stress.

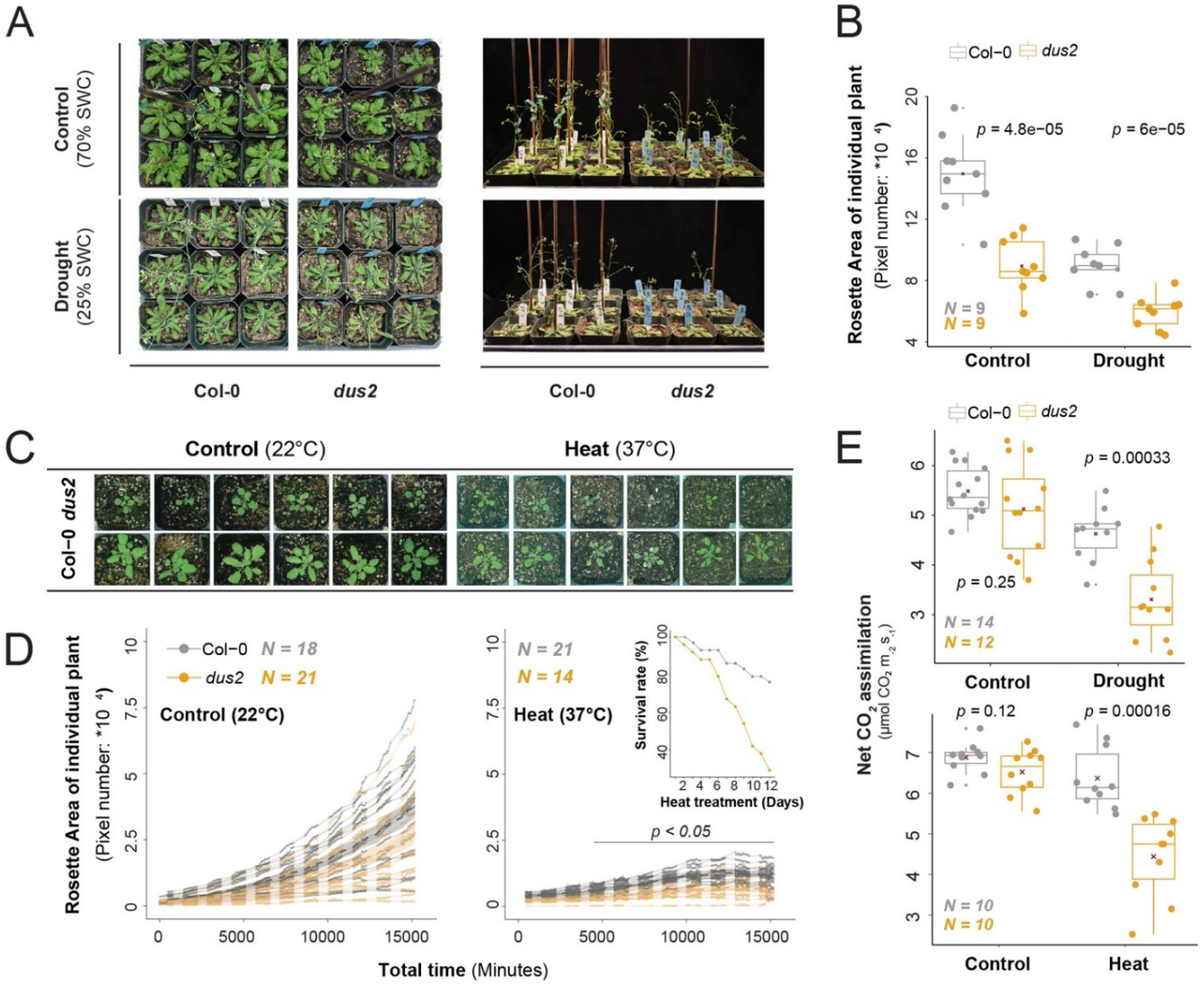

Figure 5. Examination of abiotic stress response between Col-0 and *dus2* in Arabidopsis
(A) Arabidopsis rosettes and seedling architecture of 4-week-old seedlings among control (70% SWC) and drought (25% SWC) conditions were displayed. **(B)** Comparison of Arabidopsis rosette area at the last day of drought treatment between Col-0 and *dus2* plants under 70% SWC and 25% SWC conditions (t-test, $p < 0.05$). **(C)** Images show Arabidopsis rosette characteristics at the 12th day of heat treatment between two genotypes. **(D)** Image-based phenotyping of Arabidopsis rosette area over 12 days of vegetative growth under control and heat conditions (30 minutes interval) processed by PlantCV (Yu et al., 2024a). Inset panel under heat depicts survival rates over time. **(E)** Photosynthetic efficiency (net CO_2 assimilation) was measured on the largest rosette leaf using a LI-6800 system. CO_2 net assimilation rate under heat (24h at 37°C) and control (22°C), control (70% SWC) and drought (25% SWC) were measured with more than 10 replicates per genotype per condition.

Heat stress induces pronounced alterations in mRNA stability in Atdus2

Next, we aimed to understand the DHU-dependent molecular responses that make the *Atdus2* background less robust under abiotic stress. For this, we profiled *AtDUS2*-dependent transcripts and DHU abundance, as well as RNA-decay changes that occur in response to heat stress in Arabidopsis.

796 Heat stress, rather than water withholding, was applied as it is both easier to apply consistently and
797 quantitatively and it can be applied to seedlings in the RNA-decay experimental framework. In addition,
798 our data indicated that *Atdus2* mutants showed diminished growth/survival at both the seedling and
799 vegetative rosette stages under heat stress (**Figures 5D** and **S4D**). We monitored DHU abundance using
800 HAMR/Modtect RCM calling of Illumina RNA-seq collected daily over a period of four days following
801 implementation of heat stress (N = 8 per genotype and condition). An examination of these data revealed
802 significantly increased mean DHU levels in Col-0, but not in *Atdus2*, in plants exposed to heat stress
803 relative to their appropriate controls (**Figure 6A**, p = 0.048 and p = 0.88, respectively), suggesting that
804 DHU is a standard mRNA-level stress response. As expected, we also observed a significant heat-stress
805 associated increase in the other HAMR/Modtect identifiable RCMs in both Col-0 and *Atdus2* backgrounds
806 (**Figure 6A**, p = 0.037 and p = 0.024, respectively). These data indicate a heat-dependent shift in DHU
807 profiles that is dependent on *AtDUS2*.

808 We then profiled the transcriptomic changes that occurred in these two backgrounds following
809 heat stress. A total of 3,186 and 3,259 transcripts (**Table S14**) were differentially abundant in Col-0 and
810 *Atdus2*, respectively, between control and heat stress conditions (FDR < 0.05, $|\log_2 FC|$ > 1; **Figure S9A**
811 **and S9C**). As expected, the transcripts up-regulated in both backgrounds (**Figure S9B**, grey bars) were
812 enriched for stress response-related terms, indicating the applied stress was sufficient to elicit a response
813 However, terms enriched in the set of Col-0 specifically upregulated transcripts suggest that it is mounting
814 a response to DNA damage, recombinational repair, and slowing down cell division, whereas the *Atdus2*
815 mutant exhibited an increase in jasmonic acid related terms and a decrease in salicylic acid and
816 photosynthesis-related terms (**Figure S9D**). To elucidate genotypic-specific stress response due to
817 *Atdus2* loss-of-function, we profiled the unique transcripts that were differentially abundant in response
818 to heat stress (**Figure S7C**). Particularly, these are subset of transcripts that exhibited a strong stress
819 response in the Col-0 but were unaltered in the *Atdus2* background (**Figure S7C**, red boxes), suggesting
820 that a functional DUS2 was necessary for their heat-associated response. We profiled the top three non-
821 redundant KEGG and GO terms of transcripts either up or down-regulated in Col-0 in response to heat
822 (**Figure S7D**). As expected, photosynthesis was the top enriched KEGG and GO term in the down-
823 regulated transcripts in Col-0 in response to heat. In sum, these data suggest that Arabidopsis DUS2 is
824 necessary for an appropriate DHU-mediated stress response, with photosynthesis-related traits and
825 transcripts the primary target.

826 To further explore the mechanism driving the increased stress susceptibility observed in the
827 *Atdus2* background, we next assessed if DHU-associated changes might influence RNA stability during
828 heat stress. To assess RNA stability, seven-day-old seedlings in ½ MS liquid culture were acclimated at
829 37°C for 12 hours, and then treated with cordycepin, with samples collected over six hours as we did

under control condition (**Figure S6B**). Global profiling of mRNA decay rates for the 12,450 model-fitted transcripts (**Table S12**) revealed that, in response to heat stress, a substantial proportion of mRNAs exhibited longer half-lives in *Atdus2* compared with Col-0 under both conditions (~47% under control and 51.6% under heat ($\log_2$FC(half-life ratio) > 0.1; **Figure 6B**). We than focused on transcripts with detectable DHU in Col-0 under heat stress. Using the HAMR/Modtect approach, we identified a total of 357 DHU-modified transcripts in Col-0 under heat, 213 of which showed reduced DHU in *dus2* (**Table S12**). Further selecting for transcripts with fitted decay models, we obtained 135 transcripts for comparison. For these transcripts, we observed significantly reduced decay rates (*K*) under heat in the *Atdus2* background (p = 1.3e-06, blue boxplots) that was not evident for non DHU-modified transcripts (red boxplots; **Figure 6C, left**, p = 0.88). This result is consistent with the cumulative frequency of half-lives, where transcripts associated with reduced DHU level in *Atdus2* exhibited significantly shorter half-lives in Col-0 than *dus2* (p= 1.83e-05, blue lines). In contrast, the half-lives of non-DHU modified transcripts remained unchanged between the two genetic backgrounds (**Figure 6C, right,** p = 0.0744, red lines).

A closer examination of these 135 transcripts using clustering heatmap uncovered three groups of transcripts with differentiated decay profiling (**Figure 6D**). More than half of transcripts (N = 78) exhibited substantially reduced half-lives in Col-0 relative to *Atdus2* in response to heat stress (**Figure 6D and Figure S8A**, average half-lives denoted for each cluster), whereas the remaining 57 transcripts exhibited increased half-lives in Col-0 under heat. In control settings, the DHU-modified transcripts with increased half-lives in the *Atdus2* background were enriched for the expected photosynthetic terms (N = 125, **Figure S8B**, top). Photosynthetic terms were also enriched for the pool of 78 DHU-modified transcripts with increased half-lives under heat in the *Atdus2*, but were also accompanied by abiotic stress terms (**Figure S8B,** bottom). Of the 78 DHU-modified transcripts that displayed a longer half-life in the *Atdus2* mutants relative to Col-0 under heat stress, 33 were associated with photosynthesis terms, including common photosystem I and II-associated transcripts, (eg., LHCA, LHCB, and PSB transcripts). Indeed, these transcripts had some of the largest half-life shifts, ranging from 2-100x longer (**Figure 6E**), indicating that DHU is necessary for their faster turnover in Col-0. In sum, these data suggest that the diminished performance under heat stress is likely due to impaired turnover of these photosynthesis-related transcripts and point to a novel post-transcriptional regulatory mechanism for these critical genes.

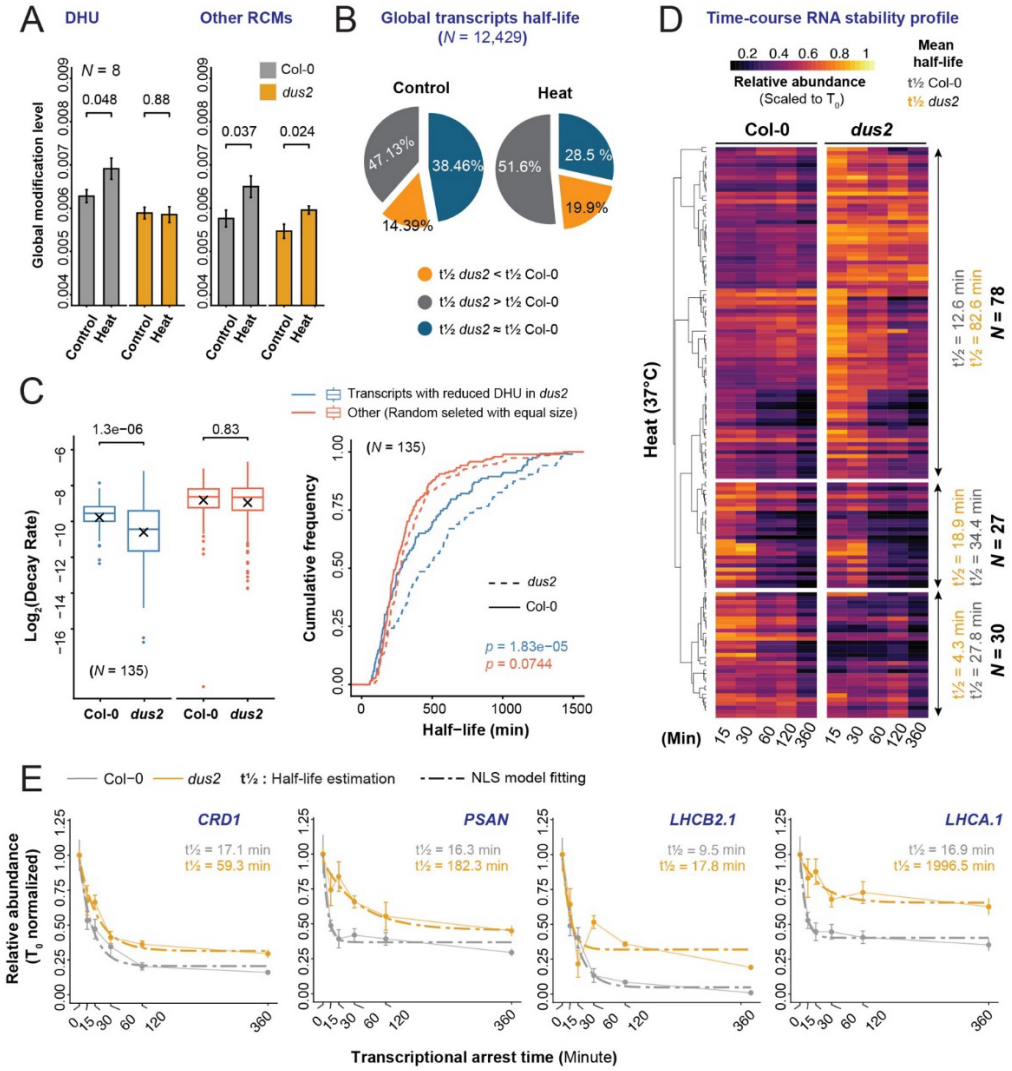

Figure 6. Comparison of abiotic stress-induced RNA stability between Col-0 and *dus2*

(A) A total of 12,450 transcripts with fitted half-life model were compared across two genotypes and two conditions, classified into six groups with respective proportions displayed using pie charts. Each group was classified based on $\log_2$FoldChange(half-life) based on exponential model fitting. **(B)** Left: Decay rate (*K*) based on exponential modeling on groups of transcripts with lower DHU level in *dus2* mutants under heat condition (blue boxplots) was compared with subset of randomly selected transcripts with equal sample size (red boxplots) using t-test ($p < 0.05$). Right: Cumulative frequency of estimated half-life of transcripts in Col-0 (solid line) and *dus2* (dashed line) background with lower DHU level in *dus2* mutants (blue lines) were compared with randomly selected transcripts (red lines) under heat stress. **(C)** Heatmap of 20 transcripts associated with differential DHU, transcript abundance, and protein abundance was plotted. Boxplots show GMUCT and RNA modification level of 16 transcripts with reduced protein in Col-0 relative to *dus2* (Wilcox test, $p < 0.05$). **(D)** Heatmap of 18 transcripts associated with differential DHU under both 22°C and 37°C conditions (left), protein class (photosystem I/II) were indicated with yellow and green box, Blue/grey colored boxes along the right indicate whether the Arabidopsis transcripts have a DHU modified ortholog in sorghum, and whether that transcript was assigned to the "blue" module or not (grey). **(E)** Box plot of DHU level and other RCM level in Col-0 (grey) and *dus2* mutants (orange) under the two conditions (t.test, $p < 0.05$). **(F)** Estimated RNA half-life of 15/18 transcripts with differentiated DHU level and degradation in Col-0 and *dus2*, facet by genotypes, with half-life estimated using exponential model and compared among four groups (Wilcox test, $p < 0.05$).

878 ## Discussion

879 Drought and heat are common abiotic stressors that induce complex phenotypic and molecular
880 responses that often lead to reduced photosynthesis, biomass, and seed set, thereby adversely affecting
881 the overall productivity of agricultural crops. Sorghum's adaptation to heat and drought makes its genetic
882 and phenotypic diversity useful for revealing regulatory mechanisms that enable maximal growth under
883 diverse field conditions. Although a variety of stress-responsive genes have been identified in sorghum
884 and other stress resilient plant species (Pardo and VanBuren, 2021; Pardo et al., 2023), gaps remain,
885 particularly in post-transcriptional regulatory events that have been shown to impact performance in other
886 species.

887 To connect differences in plant performance in the field to specific transcriptional and post-
888 transcriptional regulatory events, we performed a multi-omic comparison of six diverse sorghum
889 accessions grown under water limiting and control conditions. We integrated molecular and physiological
890 variation in a systems-level analysis to identify potential causal factors. As expected, physiological
891 parameters and genes associated with photosynthesis, water movement, and stress-response regulation
892 were all impacted to varying degrees in our panel (**Figure 1**). Interestingly, we also observed variation in
893 one of the RCMs that we were able to be detected through standard Illumina RNA-sequencing
894 approaches, DHU, that was strongly correlated with transcript abundance and plant performance in the
895 six accessions (**Figure 2A**). Furthermore, our co-expression network analysis identified a dihydrouridine
896 synthase (*SbDUS2*) transcript that was also associated with photosynthesis traits and DHU status of
897 related transcripts. Importantly, the correlation between *SbDUS2* expression and the suite of transcripts
898 with predicted DHU sites was observed in other public datasets and was not unique to our specific field
899 conditions, growth parameters, or accessions. Thus, SbDUS2 and DHU appear to be linked with
900 transcript groups associated with physiological traits.

901 While RCMs have been shown to influence or be associated with plant stress responses (Yu et
902 al., 2021; Sharma et al., 2023; Cai et al., 2025), the identification of SbDUS2 associated with
903 photosynthesis and stress-related transcripts was nevertheless a surprise. The DHU modification is
904 mostly associated with tRNAs, and indeed the DUS protein family is conserved across the tree of life,
905 including in eukaryotes, prokaryotes, and some archaea (Yu et al., 2011; Finet et al., 2022a; Finet et al.,
906 2022b). Due to advances in detection capabilities, DHU has recently been described on mRNAs in
907 humans and yeast (Dai et al., 2021; Finet et al., 2022b; Draycott et al., 2022), where it has been reported
908 to influence splicing, translation, and fundamental biological processes such as meiosis (Finet et al.,
909 2022b). Using computational algorithms that infer DHU status based on non-random errors introduced
910 during the RT-PCR step of RNA-seq library preparation, we were also able to predict DHU-marked
911 transcripts, and indeed our data suggest that these transcripts were enriched for a set of photosynthesis,

912 metabolism, and other fundamental cellular processes. Whether this is due to sequence intrinsic features,
913 functional conservation, or speculatively is an ancient organellar feature from before they were
914 incorporated into the nuclear genome, is unclear and will likely guide future discoveries. The enrichment
915 of predicted DHU on these highly abundant transcripts, may also be due to detection biases that scale
916 with abundance. Monitoring DHU at the transcript level, or on lowly abundant transcripts, will likely only
917 be possible with technical advances, such as ONT's direct RNA-seq, and associated detection algorithms.
918 Given that this was the first detailed study of DHU in plants, and in particular on how DHU might
919 contribute to plant growth and development, we sought to develop a clearer picture of how DHU is
920 performing this function by examining Arabidopsis lines with the orthologous *Dus2* locus disrupted. Using
921 LC-MS/MS, we confirmed that DHU levels were reduced in total RNA derived from *Atdus2* mutants
922 relative to the Col-0 controls. Since we expected much of this DHU signal to be associated with the more
923 abundant tRNA class, we also specifically examined mRNA-associated DHU levels using both
924 HAMR/Modtect on Illumina RNA-seq and by comparing Nanopore DRS between WT (Col-0) and *Atdus2*
925 mutants. We observed a DUS2-dependent decrease in DHU levels in mRNA using these two
926 complementary approaches, suggesting that AtDUS2, like other eukaryotic DUS2 enzymes, modifies
927 mRNAs in addition to other RNA classes. With evidence supporting a DUS2-dependent reduction in
928 mRNA-associated DHU, we then assessed the impact that diminished DHU abundance had on plant
929 performance. A very real concern is that the loss of DUS2 might have pleotropic effects on plant
930 performance simply due to its potential role in modifying tRNA, thereby diminishing translation of all
931 protein classes. Importantly, untargeted protein mass spectrometry did not reveal a broad reduction in
932 protein abundance **(Figure S6**) but instead revealed a very specific reduction in proteins associated with
933 photosynthesis and metabolism, similar to the class of mRNAs associated with DHU modification.
934 Whether AtDUS2 doesn't play a prominent role in the addition of DHU to tRNAs, or if its absence is
935 compensated by one of the other four DUS enzymes in Arabidopsis, remains to be tested.
936 An examination of the transcriptomic and proteomic changes in the *Atdus2* background provided
937 clues as to what might give rise to the reduced germination and delayed development under control
938 conditions. We predominantly detected a reduction in photosynthesis-related transcripts in the *Atdus2*
939 background. Dysregulation of these transcripts could certainly explain the delayed, slower growth that
940 we observed in both Arabidopsis and in sorghum with reduced *DUS2* levels (e.g., the "A" accession), and
941 under stress or control conditions, as plants with reduced photosynthesis struggle to efficiently capture
942 and convert light energy into glucose. Interestingly, glucose, alongside other carbohydrates, were
943 strongly correlated with the photosynthesis-associated *DUS2* co-expression modules **(Figure 2A**), again
944 highlighting a model where DUS2, and DHU, are potentially critical for efficient photosynthesis.
945

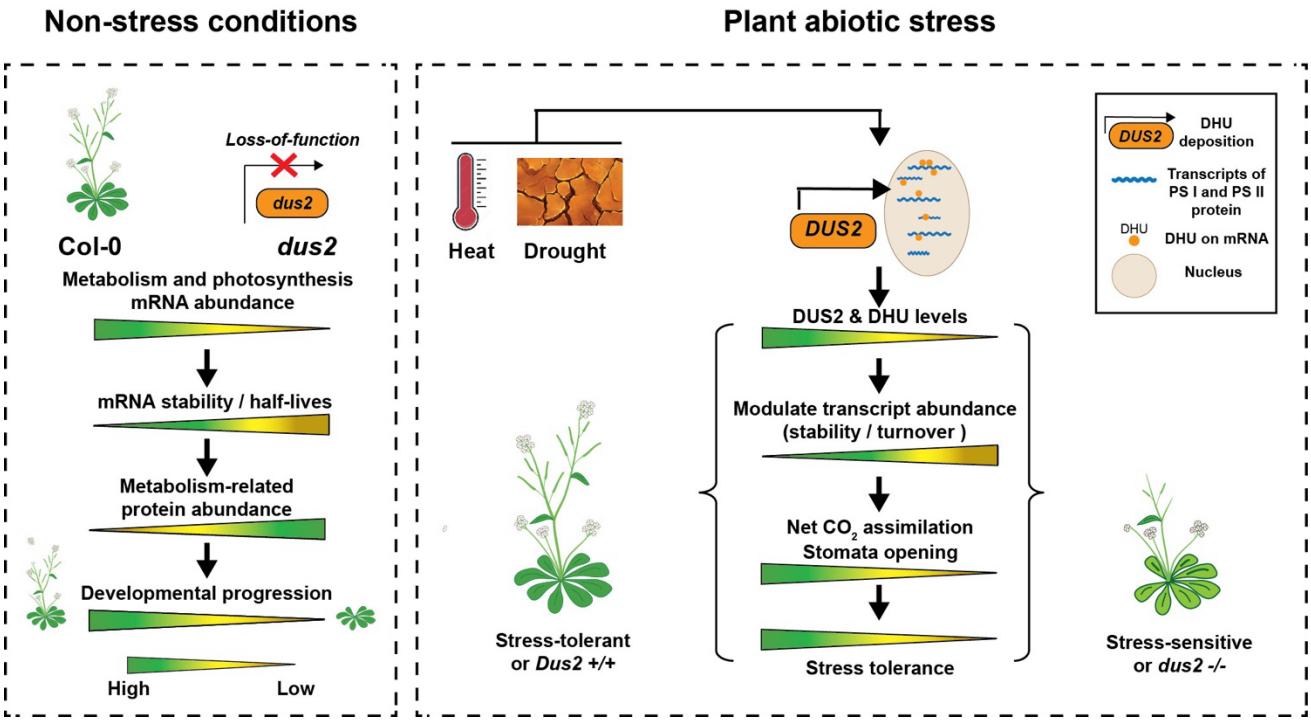

Figure 7. Proposed model explains DHU impacts on plant growth and stress response
Based on our findings in *Arabidopsis*, reduced DHU levels appear to impact the abundance of a subset of DHU-modified transcripts in Col-0. Loss of DUS2 shifts the stability and half-lives of mRNAs encoding proteins involved in photosynthesis and metabolism, which in turn leads to impaired germination and delayed growth in the mutant background. Growth defects are exacerbated when plants are grown under abiotic stress conditions, due to a proposed inappropriate turnover of photosynthesis-associated transcripts. Counterintuitively, increases in these unmodified photosynthesis-related transcripts in the Atdus2 mutant leads to reduced photosynthesis parameters, likely due to a buildup of ROS and eventual cell death. Thus, DHU is necessary to reduce mRNA steady state levels, or to target mRNAs for degradation, helping to manage the pool of photosynthesis-related proteins and ultimately allowing for better stress tolerance.

The observed impact of *AtDus2*-dependent DHU on photosynthesis were pronounced under abiotic stress conditions in Arabidopsis, with reduced *AtDUS2* levels associated with decreased plant performance. This raises the question of how a modification that appears to be negatively associated with transcript abundance could be beneficial for plant performance under stress? We propose a model, supported by RNA decay data in both Col-0 and *Atdus2* mutants under control and heat conditions, whereby DHU is likely necessary for appropriate mRNA turnover under stress conditions (**Figure 7**). The observation that DHU-associated photosynthesis transcripts exhibited substantially increased half-lives (up to 100-fold) in the Atdus2 background provides support for this model of DHU-dependent transcript destabilization. In addition, prior work examining HAMR detectable RCMs in Arabidopsis found that this group of modifications, which included DHU, were heavily enriched on actively degrading transcripts under control conditions (Vandivier et al., 2015). Higher turnover, reduced steady state levels, and structural perturbations of photosynthesis and metabolism related transcripts have been observed under

971 stress conditions in a number of plant systems (Li et al., 2022; Notarnicola et al., 2023) with these
972 changes proposed as a rapid means of clearing molecules that are accumulating damage caused by
973 reactive oxygen species (ROS; Park et al., 2012). While plants attempt to limit photosynthesis during
974 stress, as it is one of the main ROS producing mechanisms in the cell, inappropriately elevated
975 photosynthesis can lead to cell death-inducing ROS levels. We propose that DHU is an RCM that marks
976 mRNAs for degradation, thereby might helping to clear them more rapidly and facilitate a proper response
977 to environmental perturbations. Excitingly, there is a clear connection between the cytoplasmic mRNA
978 decay machinery and stress tolerance in Arabidopsis (Merret et al., 2013) and DHU, or a sufficient
979 accumulation of DHU marks, may target mRNAs towards this pathway. We propose that Arabidopsis
980 plants lacking DUS2, or that decrease DUS2 levels or activity in response to stress conditions, would
981 then be unable to clear these damaged mRNA molecules through cytoplasmic decay pathways,
982 potentially increasing cell death and diminishing plant performance.

983 In summary, our comparative, multi-species approach facilitated the identification of an RCM that
984 appears to be critical for plant performance under stress. Indeed, this RCM influences abiotic stress
985 responses in Arabidopsis by acting on many of the photosynthesis and metabolism-related mRNAs.
986 These data highlight the complex transcriptional and post-transcriptional regulatory landscape influencing
987 plant stress responses and offer promising insights as to how they might be used to select more stress-
988 resilient plants in the future.

989

990 ## Data availability

991 Transcriptome sequencing reads have been deposited in the National Center for Biotechnology
992 Information (NCBI) BioProject database under the accession number: PRJNA1119650**.** Chromatograms
993 of 5,6-dihydrouridine Mass spectrometry data was deposited under massIVE online repository
994 (ftp://massive.ucsd.edu/v09/MSV000097205/). Computational pipelines used for data analysis were
995 deposited under the GitHub page (https://github.com/Leon-Yu0320/Sorghum_Range28). The R
996 markdown files (R code) for data visualization in main figures and supplementary figures were deposited
997 in Rpubs workspace (https://rpubs.com/LeonYu/Main-Figures and https://rpubs.com/LeonYu/Supp-
998 Figures).

999

1000 ## Acknowledgments

1001 We would like to thank the members of the epitranscriptomic working group within the Nelson, Pauli,
1002 Schroeder, and Gregory labs for their insightful comments. We would like to thank Dr. Cliff Weil for
1003 insightful comments about the SAP, Dr. Tony Schilmiller and the MSU Mass Spectrometry and

1004 Metabolomics Core for assistance in metabolomics measurements and analysis. Many thanks to Dr.
1005 Alyssa Kearly for her assistance in technical proofing of the manuscript. This work was supported by NSF
1006 IOS PGRP 2023310 (to ADLN, EHL, DP, and BDG), NSF IOS PGRP 1849708 (to BDG), NSF MCB
1007 2427729 (to BDG), NSF MCB 2102120 (to ADLN and DP), Department of Energy (DOE) DE-AR0001101
1008 (to DP), DE-SC0023305 (to DP and AE), DE-SC0020401 (to AE and DP), Cotton Incorporated 18-384,
1009 20720, and 21-830 (to DP), NSF DBI-2019674 (to DP and ADLN), and NIH R35GM153298 (to AIS).

1010

1011 ## Author contributions

1012 LY, GM, AEA, EHL, BDG, ADLN, and DP developed the experiment. GM, SC, BR, and DP designed the
1013 field experiment and collected field-related data. ACND and EKB extracted RNA and performed other
1014 sorghum-related molecular experiments. AE provided accessions from the SAP for this study. LY, ApS,
1015 XZ, and EKB worked with the Arabidopsis DUS2 mutants. DRG generated and contributed to the analysis
1016 of GMUCT data. GM and TO generated the metabolomics data. HA and GB generated the biochemical
1017 data related to oxidative stress status. LY, RH, and DS helped and provided expertise in acquiring
1018 physiological measurements for the Arabidopsis DUS2 mutants. HF and AIS performed mass-spec
1019 experiments on the DUS2 mutants. LY analyzed all RNA-seq and developed co-expression networks
1020 and data integration. LY, KP, and SJS analyzed epitranscriptomic data. LY, BDG, ADLN, and DP wrote
1021 the manuscript.

Figure Legends

Main Figures

Figure 1. Drought tolerance diversity of selected sorghum genotypes
(A) Reconstruction of an unrooted phylogeny of the Sorghum Association Panel (SAP). The six sorghum accessions used in this study are marked along with the geographical locations colored to represent African (green), Asian(purple), and North American (blue) regions. The placement of the six accessions used in this study is denoted with different colored stars that match the color scheme throughout this work. (**B)** Six sorghum accessions were grown at the Arizona in the field with treatment (reduced water supply) imposed 47 days after planting (DAP). Paired molecular sampling (RNA-seq, metabolites, and oxidative stress chemicals), were collected alongside physiological measurements (e.g., LI-6800 photosynthesis-related traits). **(C)** Representative leaf tissue collected at the terminal stage of sampling in the field is shown. **(D)** Line graphs denote the mean WUEi and internal CO_2 concentration values measured during the morning (top) and afternoon (bottom) at each time point for drought-treated plants (N = 5 per accession). Asterisks indicate significant differences of parameters derived from the comparison of each accession relative to "A" ($p < 0.05$). **(E)** Two principal component analyses (PCAs), based on the top 10% most abundant transcripts, highlight the separation caused by genotypic and treatment effects (left) and genotypic and temporal effects (right). **(F)** The left PCA displays separation based on treatment (triangle = drought; circle = control) and genotype (colors similar to those in panel C). The right PCA loading plot highlights major contributors to the left PCA, with the length of the line denoting the contribution of a particular molecule to the PCA.

Figure 2. Selection of co-expression modules contributing to sorghum drought tolerance
(A) The number of transcripts per module, correlation between traits and the module (blue and red scale), levels of KEGG and GO enrichment levels (purple and brown scale), and the known proteins related to RCM recognition, deposition, and removal located in each co-expression module. Scales for module-trait correlation values (blue to red scale: -1 to 1), as well as GO-enrichment levels (purple to yellow scale: fold changes) are shown to the bottom left. Only those module-trait correlations and enrichment levels with a $p < 0.05$ are shown. **(B)** The eigenvalue of the photosynthetic module, divided by accession, treatment, and time, was plotted. (**C)** Correlation of transcript abundance and modification was compared between 326 transcripts been modified by both DHU and other RCMs in the blue module. **(D)** Bar plots denote the $\log_2(FDR)$ score of consensus enrichment terms, with number of genes associated with the term over the total genes in the term (middle), and the fold change for each term (right) **(E):** Box plots denote the correlation coefficient (r) between transcript abundance and each photosynthetic trait (A, Ci, and gsw) between DHU-modified group and the non-modified group. **(E)** Principal component analysis (PCA) of DHU-modified transcripts from the "blue" module (N = 326 transcripts). **(F)** Metaplot shows density of DHU sites across upstream (downstream) 250bp genomic region near start (stop) codon over 325 transcripts in accession "A" and other five accessions under control and drought conditions. (**G)** TPM of *SbDUS2* and *SbDUS3* across the two conditions and six accessions.

Figure 3. Characterization of the *dus2* mutant in Arabidopsis
(A) Schematic of the *AtDUS2* locus (top) with the T-DNA insertion sites in the third and fourth exon denoted. A protein alignment of the Arabidopsis and sorghum DUS2 proteins is depicted below, with the DUS-FMN-like domain outlined in orange. Alignment coverage and amino acid identity is shown below. **(B)** Left: Comparison of 5,6-dihydrouridine between two genetic backgrounds using LC–MS/MS analysis of hydrolyzed total RNA with external calibration using synthetic 5,6-dihydrouridine standards under (10, 50, 100 nM); Middle: Density plot of significantly modified sites (q-value < 0.05) between Col-0 and *dus2* of uridine-associated/non-uridine associated sites using Nanopore DRS**. (C)** Quantification based on imaging of seeds grown on MS plates, with each datapoint representing three plates. Germination was calculated as the full emergence of cotyledons with images after 2-day germination **(D)** Top-view images

of two independent dus2 T-DNA insertion lines at 2-week of growth (left). Side images of the two backgrounds at the point of silique maturation for Col-0 (36 days; top), and top-view images of the rosettes captured at the same timepoint (bottom).

Figure 4. Altered RNA stability between Col-0 and *dus2* background

(A) Boxplot shows comparison of GMUCT-derived uncapped portions per transcripts over transcripts associated with lower DHU level in *dus2* (blue boxplots) and other transcripts (red boxplots) in Col-0 and *dus2* background, examinate by Wilcox test. **(B)** Decay rate (*K*) on groups of transcripts with lower DHU level in *dus2* mutants (blue boxplots) were compared with subset of randomly selected transcripts with equal sample size (red boxplots) using t-test ($p < 0.05$) on the left; Cumulative frequency of estimated half-life of transcripts in Col-0 (solid line) and *dus2* (dashed line) background with lower DHU level in *dus2* mutants (blue lines) were compared with randomly selected transcripts (red lines) on the right. **(C)** Heatmaps show differentiated decay rate of transcripts derived from panel (B), which majority faster decay in Col-0, partial similar decay between two genotypes, and small groups with slower decay in Col-0 under both control and heat conditions. **(D)** Heatmap of 20 transcripts associated with differential DHU, transits abundance, and protein abundance was plotted. Boxplots show GMUCT and RNA modification level of 16 transcripts with reduced protein in Col-0 relative to *dus2* (Wilcox test, $p < 0.05$), along with estimated half-life comparison of14/16 transcripts (Wilcox test). **(E)** RNA decay curve 6-hour experiment and line graph (error bars displayed) of four selected transcripts associated with higher DHU level and faster degradation in Col-0 than *dus2*, with estimated half-life were using NLS model.

Figure 5. Examination of abiotic stress response between Col-0 and *dus2* in Arabidopsis

(A) Arabidopsis rosettes and seedling architecture of 4-week-old seedlings among control (70% SWC) and drought (25% SWC) conditions were displayed. **(B)** Comparison of Arabidopsis rosette area at the last day of drought treatment between Col-0 and *dus2* plants under 70% SWC and 25% SWC conditions (t-test, $p < 0.05$). **(C)** Images show Arabidopsis rosette characteristics at the 12th day of heat treatment between two genotypes. **(D)** Image-based phenotyping of Arabidopsis rosette area over 12 days of vegetative growth under control and heat conditions (30 minutes interval) processed by PlantCV (Yu et al., 2024a). Inset panel under heat depicts survival rates over time. **(E)** Photosynthetic efficiency (net CO_2 assimilation) was measured on the largest rosette leaf using a LI-6800 system. CO_2 net assimilation rate under heat (24h at 37°C) and control (22°C), control (70% SWC) and drought (25% SWC) were measured with more than 10 replicates per genotype per condition.

Figure 6. Comparison of abiotic stress-induced RNA stability between Col-0 and *dus2*

(A) A total of 12,450 transcripts with fitted half-life model were compared across two genotypes and two conditions, classified into six groups with respective proportions displayed using pie charts. Each group was classified based on $\log_2$FoldChange(half-life) based on exponential model fitting. **(B)** Left: Decay rate (*K*) based on exponential modeling on groups of transcripts with lower DHU level in *dus2* mutants under heat condition (blue boxplots) was compared with subset of randomly selected transcripts with equal sample size (red boxplots) using t-test ($p < 0.05$). Right: Cumulative frequency of estimated half-life of transcripts in Col-0 (solid line) and *dus2* (dashed line) background with lower DHU level in *dus2* mutants (blue lines) were compared with randomly selected transcripts (red lines) under heat stress. **(C)** Heatmap of 20 transcripts associated with differential DHU, transcript abundance, and protein abundance was plotted. Boxplots show GMUCT and RNA modification level of 16 transcripts with reduced protein in Col-0 relative to *dus2* (Wilcox test, $p < 0.05$). **(D)** Heatmap of 18 transcripts associated with differential DHU under both 22°C and 37°C conditions (left), protein class (photosystem I/II) were indicated with

yellow and green box, Blue/grey colored boxes along the right indicate whether the Arabidopsis transcripts have a DHU modified ortholog in sorghum, and whether that transcript was assigned to the "blue" module or not (grey). **(E)** Box plot of DHU level and other RCM level in Col-0 (grey) and *dus2* mutants (orange) under the two conditions (t.test, $p < 0.05$). **(F)** Estimated RNA half-life of 15/18 transcripts with differentiated DHU level and degradation in Col-0 and *dus2*, facet by genotypes, with half-life estimated using exponential model and compared among four groups (Wilcox test, $p < 0.05$).

Figure 7. Proposed model explains DHU impacts on plant growth and stress response
Based on our findings in *Arabidopsis*, reduced DHU levels appear to impact the abundance of a subset of DHU-modified transcripts in Col-0. Loss of DUS2 shifts the stability and half-lives of mRNAs encoding proteins involved in photosynthesis and metabolism, which in turn leads to impaired germination and delayed growth in the mutant background. Growth defects are exacerbated when plants are grown under abiotic stress conditions, due to a proposed inappropriate turnover of photosynthesis-associated transcripts. Counterintuitively, increases in these unmodified photosynthesis-related transcripts in the Atdus2 mutant leads to reduced photosynthesis parameters, likely due to a buildup of ROS and eventual cell death. Thus, DHU is necessary to reduce mRNA steady state levels, or to target mRNAs for degradation, helping to manage the pool of photosynthesis-related proteins and ultimately allowing for better stress tolerance.

Supplementary Figures

Figure S1. Genomic composition of variants of six sorghum accessions: 8,725,449 variants (SNPs and INDELs) derived from variants calling (GATK4, reference genome: **McCormick et al., 2018)** were annotated based on genomic classifications using VEP tool, the unique variants of each accession were calculated across upstream, downstream, intron, and splicing regions.

Figure S2. Maximum likelihood phylogeny of plant and budding yeast DUS proteins
A maximum likelihood phylogeny was inferred from a protein alignment of three DUS genes identified in Arabidopsis (AT), Sorghum (Sobic), Oryza sativa (rice, Os), Physcomitreum patens (Pp), and Saccharomyces cerevisiae (Sc) through reciprocal best BLASTp. Values at each node represent bootstrap support (out of 100 replicates).

Figure S3. Features of co-expression modules in sorghum field data
(A) A child network (N = 48) was displayed by including two DUS genes (orange box) and intersected genes derived from 326 DHU-modified transcripts and photosynthesis and metabolic pathway enriched genes (N = 96). Transcripts with a correlation between DHU level and transcript abundance were marked in light blue (N = 29), with orange dashed lines connecting DUS-derived connections and light red dashed lines indicating known protein-protein interactions from the STRING database. **(B)** Heat map of 29 transcripts that displayed a negative correlation between DHU and transcript abundance. Correlation between DHU and transcript abundance is shown across the top of the heatmap, with the correlation between DUS2/3 and DHU modified transcript abundance shown along the bottom. **(C)** Examination of expression for these 29 transcripts and *SbDUS2*/*SbDUS3* in sorghum tissues or developmental stages using publicly available tissue expression atlas data from McCormick et al., 2018. Correlation between DHU and transcript abundance is shown across the top of the heatmap, with the correlation between DUS2/3 and DHU modified transcript abundance shown along the bottom. **(D)** Normalized transcript abundance (TPM) values of DUS2 and DUS2 in the sorghum public tissue atlas**. (E)** Pearson correlation between SbDUS2/3 transcript abundance relative to the PC1 score of the PCA derived from DHU-level of 326 DHU-modified transcripts in "blue" module. **(F)** The TPM level of *SbDUS1* transcripts in sorghum drought experiment.

Figure S4. Characterization of *Atdus2* mutants

(A) Illumina-mapped reads and DRS reads from DUS2 mutants and Col-0 background were visualized using the IGV tool to confirm mutant samples contain homozygous T-DNA insertion that disrupts the expression of full-length *DUS2*. **(B)** Illustration of water holding experiment to maintain certain soil water content over drought treatment. **(C)** Drought stress on 4-week Arabidopsis plants at 70% SWC or 25% SWC over time using Col-0 and two independent *dus2* mutant lines (CS857388 and SALK_079129C). **(D)** Heat stress on 7-day-old Arabidopsis seedlings grown on MS plates under control condition and prolonged heat stress 37°C (48 hours) using Col-0 and two independent *dus2* mutant lines (CS857388 and SALK_079129C). **(E)** Bud initiation rate of Col-0 and *Atdus2* plants: Percent of plants with flower buds visible plotted over time are recorded. **(F)** The plant architecture of Col-0 and *Atdus2* plants at about 50 days of growth.

Figure S5. DHU deposition characteristics in sorghum and Arabidopsis

(A) Frequencies of all 3-nt sequence combinations adjacent to DHU-modified sites (red) in sorghum and *Arabidopsis* are summarized. U-tract sites are defined as those containing at least one adjacent U near the DHU position. **(B)** Metaplots showing the distribution of DHU-modified sites in sorghum and *Arabidopsis* across the 5′UTR (±250 bp), 3′UTR (±250 bp), and full transcript bodies.

Figure S6. Molecular features of DHU-modified transcripts in Arabidopsis

(A) The volcano plot shows up and downregulated transcripts in the mutant background. **(B)** The volcano plot shows proteins associated with increased and decreased abundance in the mutant background. **(C)** Log_2FC (*dus2*/Col-0) of 275 transcripts and proteins were plotted to show correlation between transcripts and proteins, the DHU modified transcripts were marked in “dark yellow” box. **(D)** Log_2FC (*dus2*/Col-0) of DHU and protein abundance were plotted to show correlation between DHU and protein level. **(E)** Protein abundance (based on MS) and transcript abundance (RNA-seq) derived from paired samples. Only genes observed in RNA-seq, MS, and for which DHU sites can be inferred, are shown. Red dashed box highlights transcripts with increased abundance in *Atdus2*. **(F)** Density plot of exon-exon junction footprint of GMUCT data.

Figure S7. Heat-induced transcriptome response and RNA stability assay

(A) Cumulative frequency plot presents the distribution of the log_2FC(*dus2*/Col-0) of transcripts with lower DHU level in *dus2* background relative to other transcripts under control and heat conditions. *p*-value was obtained using a two-sided Wilcoxon rank sum test. **(B)** 7-day-old seedling of two Arabidopsis genotypes were grown on ½ MS media and transformed to liquid media for 12-hour incubation under 22°C and 37°C conditions. Samples were collected at various time points (0, 15, 30, 60, 120, 360 min) after cordycepin treatment for RNA extraction and sequencing **(F)** Upset plot displaying the number of all up- or down-regulated heat-induced transcripts in Col-0 and *dus2* genotypes, with red boxes highlight transcript present uniquely in one genotype at certain condition **(G)** KEGG and GO term enrichment ($-log_{10}$ *FDR*) of Col-0-specific DATs (from panel G). Only the top three terms are shown for up or down-regulated transcripts, with the number of enriched transcripts relative to the total transcripts shown in, or adjacent, to each box.

1211 **Figure S8. Heat-induced transcriptome response in Col-0 and *Atdus2* plants**
1212 **(A)** The volcano plot shows up and downregulated transcripts (heat / control) in the wildtype plants. **(B)**
1213 The bar plots show -$\log_{10}$(*FDR*) and the number in red display fold enrichment of each 10 enriched terms
1214 involved in biological processes. **(C)** The volcano plot shows up and downregulated transcripts (heat /
1215 control) in mutant plants. **(D)** The bar plots show -$\log_{10}$(*FDR*) and the number in red display fold
1216 enrichment of each 10 enriched terms involved in biological processes.
1217
1218 **Figure S9. RNA stability and GO enrichment of subset transcripts under two conditions**
1219 (A) NLS modeling of subset transcripts derived from 216 (135) transcripts with reduced DHU level in *dus2*
1220 background under control (heat) conditions. Each three groups under control and heat conditions were
1221 divided based on clustering of decay profile of transcripts. (B) GO enrichment of two larger group of
1222 transcripts with faster decay in Col-0 than *dus2* (*N* = 125 under control conditions and *N* = 78 under heat
1223 conditions).

References

Abreha, K. B., Enyew, M., Carlsson, A. S., Vetukuri, R. R., Feyissa, T., Motlhaodi, T., Ng'uni, D., and Geleta, M. (2021). Sorghum in dryland: morphological, physiological, and molecular responses of sorghum under drought stress. *Planta* **255**:20.

Aebi, H. (1984). [13] Catalase in vitro. *Methods Enzymol.*

Alizadeh, M. R., Adamowski, J., Nikoo, M. R., AghaKouchak, A., Dennison, P., and Sadegh, M. (2020). A century of observations reveals increasing likelihood of continental-scale compound dry-hot extremes. *Sci. Adv.* **6**:eaaz4571.

Anderson, S. J., Kramer, M. C., Gosai, S. J., Yu, X., Vandivier, L. E., Nelson, A. D. L., Anderson, Z. D., Beilstein, M. A., Fray, R. G., Lyons, E., et al. (2018). N6-methyladenosine inhibits local ribonucleolytic cleavage to stabilize mRNAs in Arabidopsis. *Cell Rep.* **25**:1146-1157.e3.

Arribas-Hernández, L., Bressendorff, S., Hansen, M. H., Poulsen, C., Erdmann, S., and Brodersen, P. (2018). An m6A-YTH module controls developmental timing and morphogenesis in Arabidopsis. *Plant Cell* **30**:952–967.

Benzie, I., and Strain, J. (1999). Ferric reducing/antioxidant power assay: direct measure of total antioxidant activity of biological fluids and modified version for simultaneous measurement of total antioxidant power and ascorbic acid concentration. *Methods Enzymol.* **299**:15–27.

Boatwright, J. L., Sapkota, S., Jin, H., Schnable, J. C., Brenton, Z., Boyles, R., and Kresovich, S. (2022). Sorghum Association Panel whole-genome sequencing establishes cornerstone resource for dissecting genomic diversity. *Plant J.* **111**:888–904.

Bolger, A. M., Lohse, M., and Usadel, B. (2014). Trimmomatic: a flexible trimmer for Illumina sequence data. *Bioinformatics* **30**:2114–2120.

Boyles, R. E., Brenton, Z. W., and Kresovich, S. (2019). Genetic and genomic resources of sorghum to connect genotype with phenotype in contrasting environments. *Plant J.* **97**:19–39.

Brazel, A. J., Manoj, N. S., Turck, F., and Ó'Maoiléidigh, D. S. (2025). Measuring CO2 assimilation of Arabidopsis thaliana whole plants and seedlings. *Plant Sci.* **350**:112295.

Burgess, S. J. (2023). QIAGEN RNeasy Plant RNA Extraction Protocol (Modified).

Cai, J., Shen, L., Kang, H., and Xu, T. (2025). RNA modifications in plant adaptation to abiotic stresses. *Plant Commun.* **6**:101229.

Chen, Y., Chen, L., Lun, A. T. L., Baldoni, P. L., and Smyth, G. K. (2025). edgeR v4: powerful differential analysis of sequencing data with expanded functionality and improved support for small counts and larger datasets. *Nucleic Acids Res.* **53**.

Cheng, C.-Y., Krishnakumar, V., Chan, A. P., Thibaud-Nissen, F., Schobel, S., and Town, C. D. (2017). Araport11: a complete reannotation of the Arabidopsis thaliana reference genome. *Plant J.* **89**:789–804.

Cheng, Q., Wang, P., Wu, G., Wang, Y., Tan, J., Li, C., Zhang, X., Liu, S., Huang, S., Huang, T., et al. (2021). Coordination of m6A mRNA methylation and gene transcriptome in rice response to cadmium stress. *Rice (N. Y.)* **14**:62.

Core Team, R. (2013). R: A language and environment for statistical computing. *Foundation for Statistical Computing, Vienna*

Cruciani, S., Delgado-Tejedor, A., Pryszcz, L. P., Medina, R., Llovera, L., and Novoa, E. M. (2025). De novo basecalling of RNA modifications at single molecule and nucleotide resolution. *Genome Biol.* **26**:38.

Dai, W., Li, A., Yu, N. J., Nguyen, T., Leach, R. W., Wühr, M., and Kleiner, R. E. (2021). Activity-based RNA-modifying enzyme probing reveals DUS3L-mediated dihydrouridylation. *Nat. Chem. Biol.* **17**:1178–1187.

Das, K., and Roychoudhury, A. (2014). Reactive oxygen species (ROS) and response of antioxidants as ROS-scavengers during environmental stress in plants. *Front. Environ. Sci.* **2**.

Demichev, V., Messner, C. B., Vernardis, S. I., Lilley, K. S., and Ralser, M. (2020). DIA-NN: neural networks and interference correction enable deep proteome coverage in high throughput. *Nat. Methods* **17**:41–44.

Dobin, A., and Gingeras, T. R. (2015). Mapping RNA-seq reads with STAR. *Curr. Protoc. Bioinformatics* **51**:11.14.1-11.14.19.

Dominissini, D., Moshitch-Moshkovitz, S., Schwartz, S., Salmon-Divon, M., Ungar, L., Osenberg, S., Cesarkas, K., Jacob-Hirsch, J., Amariglio, N., Kupiec, M., et al. (2012). Topology of the human and mouse m6A RNA methylomes revealed by m6A-seq. *Nature* **485**:201–206.

Draycott, A. S., Schaening-Burgos, C., Rojas-Duran, M. F., Wilson, L., Schärfen, L., Neugebauer, K. M., Nachtergaele, S., and Gilbert, W. V. (2022). Transcriptome-wide mapping reveals a diverse dihydrouridine landscape including mRNA. *PLoS Biol.* **20**:e3001622.

Edelheit, S., Schwartz, S., Mumbach, M. R., Wurtzel, O., and Sorek, R. (2013). Transcriptome-wide mapping of 5-methylcytidine RNA modifications in bacteria, archaea, and yeast reveals m5C within archaeal mRNAs. *PLoS Genet.* **9**:e1003602.

Fahlgren, N., Feldman, M., Gehan, M. A., Wilson, M. S., Shyu, C., Bryant, D. W., Hill, S. T., McEntee, C. J., Warnasooriya, S. N., Kumar, I., et al. (2015). A versatile phenotyping system and analytics platform reveals diverse temporal responses to water availability in Setaria. *Mol. Plant* **8**:1520–1535.

Feierabend, J., and Beevers, H. (1972). Developmental studies on microbodies in wheat leaves : I. Conditions influencing enzyme development: I. Conditions influencing enzyme development. *Plant Physiol.* **49**:28–32.

Finet, O., Yague-Sanz, C., Marchand, F., and Hermand, D. (2022a). The Dihydrouridine landscape from tRNA to mRNA: a perspective on synthesis, structural impact and function. *RNA Biol.* **19**:735–750.

Finet, O., Yague-Sanz, C., Krüger, L. K., Tran, P., Migeot, V., Louski, M., Nevers, A., Rougemaille, M., Sun, J., Ernst, F. G. M., et al. (2022b). Transcription-wide mapping of dihydrouridine reveals that mRNA dihydrouridylation is required for meiotic chromosome segregation. *Mol. Cell* **82**:404-419.e9.

Ganguly, D. R., Li, Y., Bhat, S. S., Tiwari, S., Ng, P. J., Gregory, B. D., and Sunkar, R. (2025). mRNA ADENOSINE METHYLASE promotes drought tolerance through N6-methyladenosine-dependent and independent impacts on mRNA regulation in Arabidopsis. *New Phytol.* **245**:183–199.

Garalde, D. R., Snell, E. A., Jachimowicz, D., Sipos, B., Lloyd, J. H., Bruce, M., Pantic, N., Admassu, T., James, P., Warland, A., et al. (2018). Highly parallel direct RNA sequencing on an array of nanopores. *Nat. Methods* **15**:201–206.

Ge, S. X., Jung, D., and Yao, R. (2019). ShinyGO: a graphical gene-set enrichment tool for animals and plants. *Bioinformatics*

Gilliham, M., Able, J. A., and Roy, S. J. (2017). Translating knowledge about abiotic stress tolerance to breeding programmes. *Plant J.* **90**:898–917.

Glaszmann, J. C., Kilian, B., Upadhyaya, H. D., and Varshney, R. K. (2010). Accessing genetic diversity for crop improvement. *Curr. Opin. Plant Biol.* **13**:167–173.

Gregory, B. D., O'Malley, R. C., Lister, R., Urich, M. A., Tonti-Filippini, J., Chen, H., Millar, A. H., and Ecker, J. R. (2008). A link between RNA metabolism and silencing affecting Arabidopsis development. *Dev. Cell* **14**:854–866.

Harcourt, E. M., Kietrys, A. M., and Kool, E. T. (2017). Chemical and structural effects of base modifications in messenger RNA. *Nature* **541**:339–346.

Helm, M., and Motorin, Y. (2017). Detecting RNA modifications in the epitranscriptome: predict and validate. *Nat. Rev. Genet.* **18**:275–291.

Hodges, D. M., DeLong, J. M., Forney, C. F., and Prange, R. K. (1999). Improving the thiobarbituric acid-reactive-substances assay for estimating lipid peroxidation in plant tissues containing anthocyanin and other interfering compounds. *Planta* **207**:604–611.

Jia, T., and Le, B. H. (2020). RNA stability measurements using RT-qPCR in Arabidopsis seedlings. *Bio Protoc.* **10**:e3680.

Kato, T., Daigo, Y., Hayama, S., Ishikawa, N., Yamabuki, T., Ito, T., Miyamoto, M., Kondo, S., and Nakamura, Y. (2005). A novel human tRNA-dihydrouridine synthase involved in pulmonary carcinogenesis. *Cancer Res.* **65**:5638–5646.

Khoury, C. K., Brush, S., Costich, D. E., Curry, H. A., de Haan, S., Engels, J. M. M., Guarino, L., Hoban, S., Mercer, K. L., Miller, A. J., et al. (2022). Crop genetic erosion: understanding and responding to loss of crop diversity. *New Phytol.* **233**:84–118.

Kim, D., Pertea, G., Trapnell, C., Pimentel, H., Kelley, R., and Salzberg, S. L. (2013). TopHat2: accurate alignment of transcriptomes in the presence of insertions, deletions and gene fusions. *Genome Biol.* **14**:R36.

Kim, D., Paggi, J. M., Park, C., Bennett, C., and Salzberg, S. (2019). Graph-based genome alignment and genotyping with HISAT2 and HISAT-genotype. *Nat. Biotechnol.* **37**:907–915.

Kovaka, S., Fan, Y., Ni, B., Timp, W., and Schatz, M. C. (2021). Targeted nanopore sequencing by real-time mapping of raw electrical signal with UNCALLED. *Nat. Biotechnol.* **39**:431–441.

Krueger, F. (2015). Trim Galore!: A wrapper around Cutadapt and FastQC to consistently apply adapter and quality trimming to FastQ files, with extra functionality for RRBS data.

Langfelder, P., and Horvath, S. (2008). WGCNA: an R package for weighted correlation network analysis. *BMC Bioinformatics* **9**:559.

LaPierre, N., Egan, R., Wang, W., and Wang, Z. (2019). De novo Nanopore read quality improvement using deep learning. *BMC Bioinformatics* **20**:552.

Lee, W.-C., Hou, B.-H., Hou, C.-Y., Tsao, S.-M., Kao, P., and Chen, H.-M. (2020). Widespread Exon junction complex footprints in the RNA degradome Mark mRNA degradation before steady state translation. *Plant Cell* **32**:904–922.

Leger, A., Amaral, P. P., Pandolfini, L., Capitanchik, C., Capraro, F., Miano, V., Migliori, V., Toolan-Kerr, P., Sideri, T., Enright, A. J., et al. (2021). RNA modifications detection by comparative Nanopore direct RNA sequencing. *Nat. Commun.* **12**:7198.

Levine, R., Williams, J. A., Stadtman, E. P., and Shacter, E. (1994). Carbonyl assays for determination of oxidatively modified proteins. *Methods Enzymol.* **233**:346–357.

Li, H. (2013). Aligning sequence reads, clone sequences and assembly contigs with BWA-MEM. *arXiv [q-bio.GN]* Advance Access published March 16, 2013.

Li, H. (2018). Minimap2: pairwise alignment for nucleotide sequences. *Bioinformatics* **34**:3094–3100.

Li, H., Handsaker, B., Wysoker, A., Fennell, T., Ruan, J., Homer, N., Marth, G., Abecasis, G., Durbin, R., and 1000 Genome Project Data Processing Subgroup (2009). The Sequence Alignment/Map format and SAMtools. *BIOINFORMATICS APPLICATIONS NOTE* **25**.

Li, X., Xiong, X., Wang, K., Wang, L., Shu, X., Ma, S., and Yi, C. (2016). Transcriptome-wide mapping reveals reversible and dynamic N(1)-methyladenosine methylome. *Nat. Chem. Biol.* **12**:311–316.

Li, L., Duncan, O., Ganguly, D. R., Lee, C. P., Crisp, P. A., Wijerathna-Yapa, A., Salih, K., Trösch, J., Pogson, B. J., and Millar, A. H. (2022). Enzymes degraded under high light maintain proteostasis by transcriptional regulation in Arabidopsis. *Proc. Natl. Acad. Sci. U. S. A.* **119**:e2121362119.

Li, H., Wang, G., Ye, C., Zou, Z., Jiang, B., Yang, F., He, K., Ju, C., Zhang, L., Gao, B., et al. (2025). Quantitative RNA pseudouridine maps reveal multilayered translation control through plant rRNA, tRNA and mRNA pseudouridylation. *Nat. Plants* **11**:234–247.

Liao, Y., Smyth, G., and Shi, W. (2013). featureCounts: an efficient general purpose program for assigning sequence reads to genomic features. *Bioinformatics* **30**:923–930.

Liu, H., Begik, O., Lucas, M. C., Ramirez, J. M., Mason, C. E., Wiener, D., Schwartz, S., Mattick, J. S., Smith, M. A., and Novoa, E. M. (2019). Accurate detection of m6A RNA modifications in native RNA sequences. *Nat. Commun.* **10**:4079.

Liu, K., Wang, X., Wang, J., Wang, S., Bai, H., Dong, W., Qiao, L., Jin, Q., Zhang, Z., Luo, G.-Z., et al. (2025). N 6-methyladenosine modifications stabilize phosphate starvation response-related mRNAs in plant adaptation to nutrient-deficient stress. *Nat. Commun.* **16**:4093.

Lobell, D. B., Burke, M. B., Tebaldi, C., Mastrandrea, M. D., Falcon, W. P., and Naylor, R. L. (2008). Prioritizing climate change adaptation needs for food security in 2030. *Science* **319**:607–610.

Lombard, M., Reed, C. J., Pecqueur, L., Faivre, B., Toubdji, S., Sudol, C., Brégeon, D., de Crécy-Lagard, V., and Hamdane, D. (2022). Evolutionary diversity of Dus2 enzymes reveals novel structural and functional features among members of the RNA dihydrouridine synthases family. *Biomolecules* **12**:1760.

Love, M. I., Huber, W., and Anders, S. (2014). Moderated estimation of fold change and dispersion for RNA-seq data with DESeq2. *Genome Biol.* **15**:550.

Luo, J.-H., Wang, Y., Wang, M., Zhang, L.-Y., Peng, H.-R., Zhou, Y.-Y., Jia, G.-F., and He, Y. (2020). Natural variation in RNA m6A methylation and its relationship with translational status. *Plant Physiol.* **182**:332–344.

McCormick, R. F., Truong, S. K., Sreedasyam, A., Jenkins, J., Shu, S., Sims, D., Kennedy, M., Amirebrahimi, M., Weers, B. D., McKinley, B., et al. (2018). The Sorghum bicolor reference genome: improved assembly, gene annotations, a transcriptome atlas, and signatures of genome organization. *Plant J.* **93**:338–354.

McKenna, A., Hanna, M., Banks, E., Sivachenko, A., Cibulskis, K., Kernytsky, A., Garimella, K., Altshuler, D., Gabriel, S., Daly, M., et al. (2010). The Genome Analysis Toolkit: a MapReduce framework for analyzing next-generation DNA sequencing data. *Genome Res.* **20**:1297–1303.

McLaren, W., Gil, L., Hunt, S. E., Riat, H. S., Ritchie, G. R. S., Thormann, A., Flicek, P., and Cunningham, F. (2016). The Ensembl Variant Effect Predictor. *Genome Biol.* **17**:122.

Melandri, G., AbdElgawad, H., Riewe, D., Hageman, J. A., Asard, H., Beemster, G. T. S., Kadam, N., Jagadish, K., Altmann, T., Ruyter-Spira, C., et al. (2020). Biomarkers for grain yield stability in rice under drought stress. *J. Exp. Bot.* **71**:669–683.

Merret, R., Descombin, J., Juan, Y.-T., Favory, J.-J., Carpentier, M.-C., Chaparro, C., Charng, Y.-Y., Deragon, J.-M., and Bousquet-Antonelli, C. (2013). XRN4 and LARP1 are required for a heat-triggered mRNA decay pathway involved in plant acclimation and survival during thermal stress. *Cell Rep.* **5**:1279–1293.

Meyer, K. D., Saletore, Y., Zumbo, P., Elemento, O., Mason, C. E., and Jaffrey, S. R. (2012). Comprehensive analysis of mRNA methylation reveals enrichment in 3' UTRs and near stop codons. *Cell* **149**:1635–1646.

Morris, G. P., Ramu, P., Deshpande, S. P., Hash, C. T., Shah, T., Upadhyaya, H. D., Riera-Lizarazu, O., Brown, P. J., Acharya, C. B., Mitchell, S. E., et al. (2013). Population genomic and genome-wide association studies of agroclimatic traits in sorghum. *Proc. Natl. Acad. Sci. U. S. A.* **110**:453–458.

Murashige, T., and Skoog, F. (1962). A revised medium for rapid growth and bio assays with tobacco tissue cultures. *Physiol. Plant.* **15**:473–497.

Murshed, R., Lopez-Lauri, F., and Sallanon, H. (2008). Microplate quantification of enzymes of the plant ascorbate-glutathione cycle. *Anal. Biochem.* **383**:320–322.

Nguyen, L.-T., Schmidt, H. A., von Haeseler, A., and Minh, B. Q. (2015). IQ-TREE: a fast and effective stochastic algorithm for estimating maximum-likelihood phylogenies. *Mol. Biol. Evol.* **32**:268–274.

Notarnicola, R. F., Arnold, P. A., Feng, Z.-P., Hamilton, J., Jones, A. W., Loke, S., Schwessinger, B., Nicotra, A. B., and Ganguly, D. R. (2023). Molecular signatures of heat tolerance and sensitivity in the alpine plant *Wahlenbergia ceracea* during moderate warming. *bioRxiv*

Obata, T., Witt, S., Lisec, J., Palacios-Rojas, N., Florez-Sarasa, I., Yousfi, S., Araus, J. L., Cairns, J. E., and Fernie, A. R. (2015). Metabolite profiles of maize leaves in drought, heat, and combined stress field trials reveal the relationship between metabolism and grain yield. *Plant Physiol.* **169**:2665–2683.

Palos, K., Nelson Dittrich, A. C., Lyons, E. H., Gregory, B. D., and Nelson, A. D. L. (2024). Comparative analyses suggest a link between mRNA splicing, stability, and RNA covalent modifications in flowering plants. *BMC Plant Biol.* **24**:768.

Pardo, J., and VanBuren, R. (2021). Evolutionary innovations driving abiotic stress tolerance in C4 grasses and cereals. *Plant Cell* **33**:3391–3401.

Pardo, J., Wai, C. M., Harman, M., Nguyen, A., Kremling, K. A., Romay, M. C., Lepak, N., Bauerle, T. L., Buckler, E. S., Thompson, A. M., et al. (2023). Cross-species predictive modeling reveals conserved drought responses between maize and sorghum. *Proc. Natl. Acad. Sci. U. S. A.* **120**:e2216894120.

Park, S.-H., Chung, P. J., Juntawong, P., Bailey-Serres, J., Kim, Y. S., Jung, H., Bang, S. W., Kim, Y.-K., Do Choi, Y., and Kim, J.-K. (2012). Posttranscriptional control of photosynthetic mRNA decay under stress conditions requires 3' and 5' untranslated regions and correlates with differential polysome association in rice. *Plant Physiol.* **159**:1111–1124.

Porra, R. J., Thompson, W. A., and Kriedemann, P. E. (1989). Determination of accurate extinction coefficients and simultaneous equations for assaying chlorophylls a and b extracted with four different solvents: verification of the concentration of chlorophyll standards by atomic absorption spectroscopy. *Biochim. Biophys. Acta Bioenerg.* **975**:384–394.

Prall, W., Sheikh, A. H., Bazin, J., Bigeard, J., Almeida-Trapp, M., Crespi, M., Hirt, H., and Gregory, B. (2023). Pathogen-induced m6A dynamics affect plant immunity. *Plant Cell* **35**:4155–4172.

Pryszcz, L. P., Diensthuber, G., Llovera, L., Medina, R., Delgado-Tejedor, A., Cozzuto, L., Ponomarenko, J., and Novoa, E. M. (2025). Rapid and accurate demultiplexing of direct RNA nanopore sequencing data with SeqTagger. *Genome Res.* **35**:956–966.

Purcell, S., Neale, B., Todd-Brown, K., Thomas, L., Ferreira, M. A. R., Bender, D., Maller, J., Sklar, P., de Bakker, P. I. W., Daly, M. J., et al. (2007). PLINK: a tool set for whole-genome association and population-based linkage analyses. *Am. J. Hum. Genet.* **81**:559–575.

Rider, L. W., Ottosen, M. B., Gattis, S. G., and Palfey, B. A. (2009). Mechanism of dihydrouridine synthase 2 from yeast and the importance of modifications for efficient tRNA reduction. *J. Biol. Chem.* **284**:10324–10333.

Riewe, D., Koohi, M., Lisec, J., Pfeiffer, M., Lippmann, R., Schmeichel, J., Willmitzer, L., and Altmann, T. (2012). A tyrosine aminotransferase involved in tocopherol synthesis in Arabidopsis: Tyrosine aminotransferase affecting tocopherols. *Plant J.* **71**:850–859.

Roundtree, I. A., Evans, M. E., Pan, T., and He, C. (2017). Dynamic RNA modifications in gene expression regulation. *Cell* **169**:1187–1200.

Ryvkin, P., Leung, Y. Y., Silverman, I. M., Childress, M., Valladares, O., Dragomir, I., Gregory, B. D., and Wang, L.-S. (2013). HAMR: high-throughput annotation of modified ribonucleotides. *RNA* **19**:1684–1692.

Schwitzguebel, J. P., and Siegenthaler, P. A. (1984). Purification of peroxisomes and mitochondria from spinach leaf by percoll gradient centrifugation. *Plant Physiol.* **75**:670–674.

Shannon, P., Markiel, A., Ozier, O., Baliga, N. S., Wang, J. T., Ramage, D., Amin, N., Schwikowski, B., and Ideker, T. (2003). Cytoscape: a software environment for integrated models of biomolecular interaction networks. *Genome Res.* **13**:2498–2504.

Shao, Y., Ma, J., Zhang, S., Xu, Y., and Yu, H. (2025). NERD-dependent m6A modification of the nascent FLC transcript regulates flowering time in Arabidopsis. *Nat. Plants*, doi:10.1038/s41477-025-01945-7.

Sharma, B., Prall, W., Bhatia, G., and Gregory, B. D. (2023). The diversity and functions of plant RNA modifications: What we know and where we go from here. *Annu. Rev. Plant Biol.* **74**:53–85.

Sorenson, R. S., Deshotel, M. J., Johnson, K., Adler, F. R., and Sieburth, L. E. (2018). Arabidopsis mRNA decay landscape arises from specialized RNA decay substrates, decapping-mediated feedback, and redundancy. *Proc. Natl. Acad. Sci. U. S. A.* **115**:E1485–E1494.

Tan, K.-T., Ding, L.-W., Wu, C.-S., Tenen, D. G., and Yang, H. (2021). Repurposing RNA sequencing for discovery of RNA modifications in clinical cohorts. *Sci. Adv.* **7**:eabd2605.

Tang, Y., Gao, C.-C., Gao, Y., Yang, Y., Shi, B., Yu, J.-L., Lyu, C., Sun, B.-F., Wang, H.-L., Xu, Y., et al. (2020). OsNSUN2-mediated 5-methylcytosine mRNA modification enhances rice adaptation to high temperature. *Dev. Cell* **53**:272-286.e7.

Tarasov, A., Vilella, A. J., Cuppen, E., Nijman, I. J., and Prins, P. (2015). Sambamba: fast processing of NGS alignment formats. *Bioinformatics* **31**:2032–2034.

Toubdji, S., Thullier, Q., Kilz, L.-M., Marchand, V., Yuan, Y., Sudol, C., Goyenvalle, C., Jean-Jean, O., Rose, S., Douthwaite, S., et al. (2024). Exploring a unique class of flavoenzymes: Identification and biochemical characterization of ribosomal RNA dihydrouridine synthase. *Proc. Natl. Acad. Sci. U. S. A..* **121**:e2401981121.

Vandivier, L. E., Campos, R., Kuksa, P. P., Silverman, I. M., Wang, L.-S., and Gregory, B. D. (2015). Chemical modifications Mark alternatively spliced and uncapped messenger RNAs in Arabidopsis. *Plant Cell* **27**:3024–3037.

Varoquaux, N., Cole, B., Gao, C., Pierroz, G., Baker, C. R., Patel, D., Madera, M., Jeffers, T., Hollingsworth, J., Sievert, J., et al. (2019). Transcriptomic analysis of field-droughted sorghum from seedling to maturity reveals biotic and metabolic responses. *Proc. Natl. Acad. Sci. U. S. A.* **116**:27124–27132.

von Mering, C., Huynen, M., Jaeggi, D., Schmidt, S., Bork, P., and Snel, B. (2003). STRING: a database of predicted functional associations between proteins. *Nucleic Acids Res.* **31**:258–261.

Wase, N., Abshire, N., and Obata, T. (2022). High-throughput profiling of metabolic phenotypes using high-resolution GC-MS. *Methods Mol. Biol.* **2539**:235–260.

Willmann, M. R., Berkowitz, N. D., and Gregory, B. D. (2014). Improved genome-wide mapping of uncapped and cleaved transcripts in eukaryotes--GMUCT 2.0. *Methods* **67**:64–73.

Wu, X., Liu, Y., Luo, H., Shang, L., Leng, C., Liu, Z., Li, Z., Lu, X., Cai, H., Hao, H., et al. (2022). Genomic footprints of sorghum domestication and breeding selection for multiple end uses. *Mol. Plant* **15**:537–551.

Wu, Y., Shao, W., Yan, M., Wang, Y., Xu, P., Huang, G., Li, X., Gregory, B. D., Yang, J., Wang, H., et al. (2024). Transfer learning enables identification of multiple types of RNA modifications using nanopore direct RNA sequencing. *Nat. Commun.* **15**:4049.

Yang, W., Meng, J., Liu, J., Ding, B., Tan, T., Wei, Q., and Yu, Y. (2020). The N1-methyladenosine methylome of petunia mRNA. *Plant Physiol.* **183**:1710–1724.

Yu, F., Tanaka, Y., Yamashita, K., Suzuki, T., Nakamura, A., Hirano, N., Suzuki, T., Yao, M., and Tanaka, I. (2011). Molecular basis of dihydrouridine formation on tRNA. *Proc. Natl. Acad. Sci. U. S. A.* **108**:19593–19598.

Yu, X., Sharma, B., and Gregory, B. D. (2021). The impact of epitranscriptomic marks on post-transcriptional regulation in plants **20**:113–124.

Yu, L., Sussman, H., Khmelnitsky, O., Rahmati Ishka, M., Srinivasan, A., Nelson, A. D. L., and Julkowska, M. M. (2024a). Development of a mobile, high-throughput, and low-cost image-based plant growth phenotyping system. *Plant Physiol.* Advance Access published May 3, 2024, doi:10.1093/plphys/kiae237.

Yu, L., Dittrich, A. C. N., Zhang, X., Brock, J. R., Thirumalaikumar, V. P., Melandri, G., Skirycz, A., Edger, P. P., Thorp, K. R., Hinze, L., et al. (2024b). Regulation of a single inositol 1-phosphate synthase homeologue by HSFA6B contributes to fibre yield maintenance under drought conditions in upland cotton. *Plant Biotechnol. J.* **22**:2756–2772.

Zhang, Q., Zhang, J., Shen, J., Silva, A., Dennis, D. A., and Barrow, C. J. (2006). A simple 96-well microplate method for estimation of total polyphenol content in seaweeds. *J. Appl. Phycol.* **18**:445–450.

Zhou, L., Gao, G., Tang, R., Wang, W., Wang, Y., Tian, S., and Qin, G. (2022). m6 A-mediated regulation of crop development and stress responses. *Plant Biotechnol. J.* **20**:1447–1455.

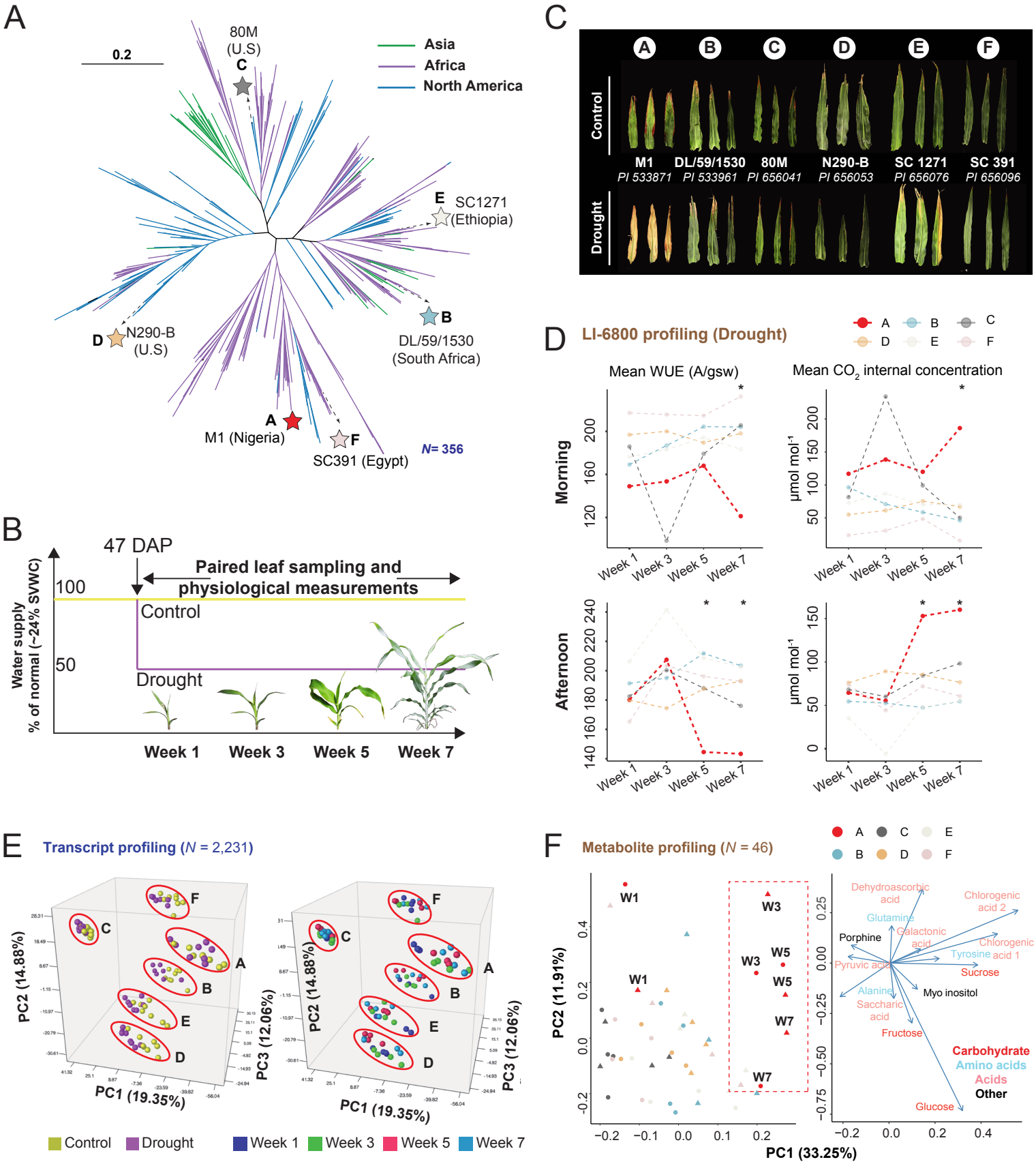
A
0.2
80M
(U.S)
C
Asia
Africa
North America
E
SC1271
(Ethiopia)
B
DL/59/1530
(South Africa)
D
N290-B
(U.S)
A
M1 (Nigeria)
F
SC391 (Egypt)
N= 356
B
47 DAP
Paired leaf sampling and
physiological measurements
100
Control
50
Drought
Water supply
% of normal (~24% SVWC)
Week 1
Week 3
Week 5
Week 7
C
A
B
C
D
E
F
Control
Drought
M1
PI 533871
DL/59/1530
PI 533961
80M
PI 656041
N290-B
PI 656053
SC 1271
PI 656076
SC 391
PI 656096
D
LI-6800 profiling (Drought)
A
B
C
D
E
F
Mean WUE (A/gsw)
Mean CO2 internal concentration
Morning
Afternoon
µmol mol-1
Week 1
Week 3
Week 5
Week 7
E
Transcript profiling (N = 2,231)
PC1 (19.35%)
PC2 (14.88%)
PC3 (12.06%)
Control
Drought
Week 1
Week 3
Week 5
Week 7
F
Metabolite profiling (N = 46)
PC1 (33.25%)
PC2 (11.91%)
W1
W3
W5
W7
Dehydroascorbic acid
Chlorogenic acid 2
Glutamine
Galactonic acid
Porphine
Chlorogenic acid 1
Tyrosine
Pyruvic acid
Sucrose
Alanine
Myo inositol
Saccharic acid
Fructose
Glucose
Carbohydrate
Amino acids
Acids
Other

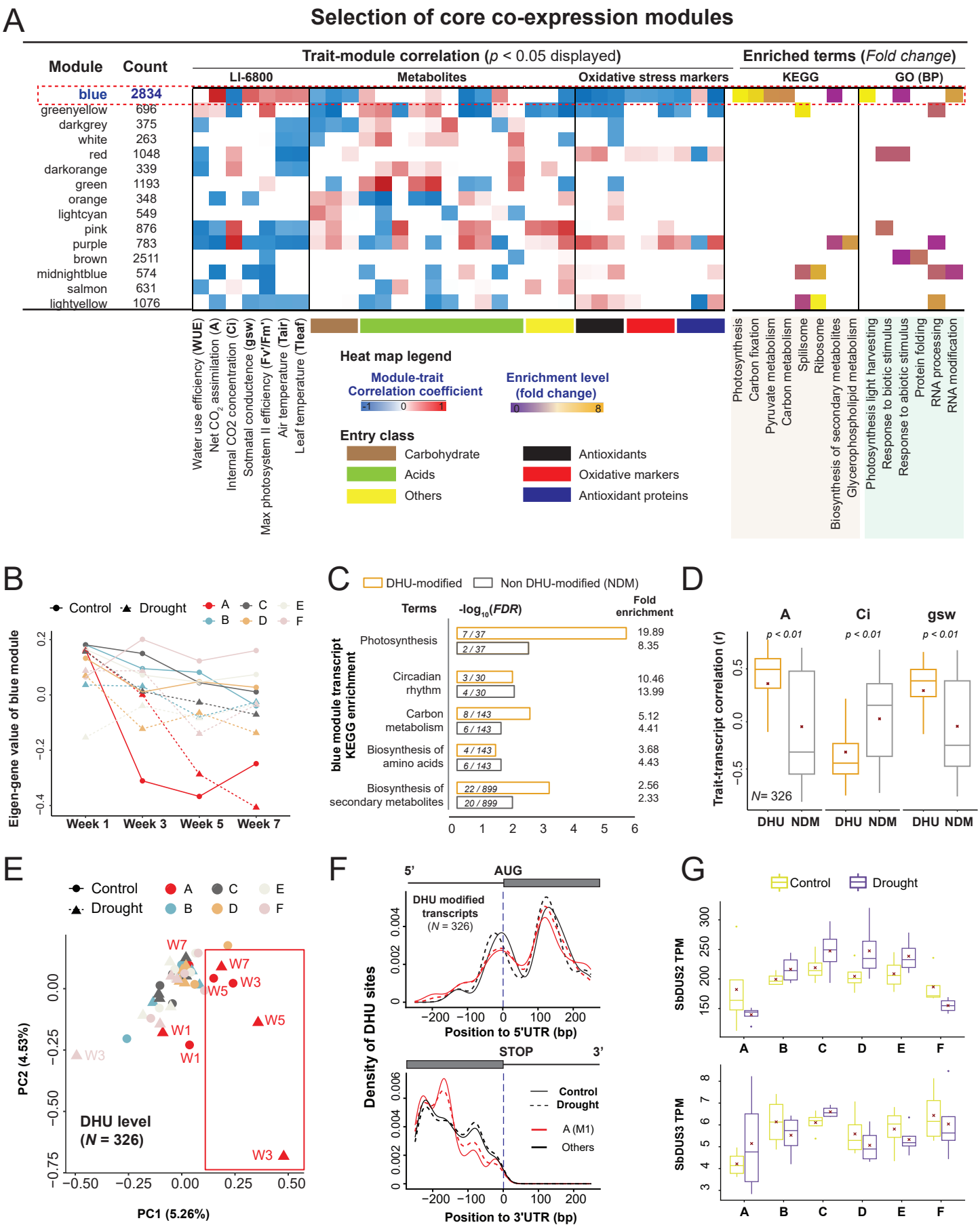
A
Selection of core co-expression modules
Module
Count
blue 2834
greenyellow 696
darkgrey 375
white 263
red 1048
darkorange 339
green 1193
orange 348
lightcyan 549
pink 876
purple 783
brown 2511
midnightblue 574
salmon 631
lightyellow 1076
Trait-module correlation (p < 0.05 displayed)
LI-6800
Metabolites
Oxidative stress markers
Enriched terms (Fold change)
KEGG
GO (BP)
Water use efficiency (WUE)
Net CO2 assimilation (A)
Internal CO2 concentration (Ci)
Sotmatal conductence (gsw)
Max photosystem II efficiency (Fv'/Fm')
Air temperature (Tair)
Leaf temperature (Tleaf)
Photosynthesis
Carbon fixation
Pyruvate metabolism
Carbon metabolism
Splilsome
Ribosome
Biosynthesis of secondary metabolites
Glycerophospholipid metabolism
Photosynthesis light harvesting
Response to biotic stimulus
Response to abiotic stimulus
Protein folding
RNA processing
RNA modification
Heat map legend
Module-trait Correlation coefficient
-1 0 1
Enrichment level (fold change)
0 8
Entry class
Carbohydrate
Acids
Others
Antioxidants
Oxidative markers
Antioxidant proteins
B
Control
Drought
A B C D E F
Eigen-gene value of blue module
0.2
0.0
−0.2
−0.4
Week 1
Week 3
Week 5
Week 7
C
DHU-modified
Non DHU-modified (NDM)
Terms
-log10(FDR)
Fold enrichment
blue module transcript KEGG enrichment
Photosynthesis
7 / 37
2 / 37
19.89
8.35
Circadian rhythm
3 / 30
4 / 30
10.46
13.99
Carbon metabolism
8 / 143
6 / 143
5.12
4.41
Biosynthesis of amino acids
4 / 143
6 / 143
3.68
4.43
Biosynthesis of secondary metabolites
22 / 899
20 / 899
2.56
2.33
0 1 2 3 4 5 6
D
A
Ci
gsw
p < 0.01
p < 0.01
p < 0.01
Trait-transcript correlation (r)
0.5
0.0
−0.5
N= 326
DHU NDM
DHU NDM
DHU NDM
E
Control
Drought
A B C D E F
W7
W3
W5
W1
DHU level
(N = 326)
PC2 (4.53%)
0.00
−0.25
−0.50
−0.75
−0.50 −0.25 0.00 0.25 0.50
PC1 (5.26%)
F
5'
AUG
DHU modified transcripts
(N = 326)
0 0.002 0.004
−200 −100 0 100 200
Position to 5'UTR (bp)
STOP
3'
Density of DHU sites
0 0.002 0.004 0.006
Control
Drought
A (M1)
Others
−200 −100 0 100 200
Position to 3'UTR (bp)
G
Control
Drought
SbDUS2 TPM
150 200 250 300
A B C D E F
SbDUS3 TPM
3 4 5 6 7 8
A B C D E F

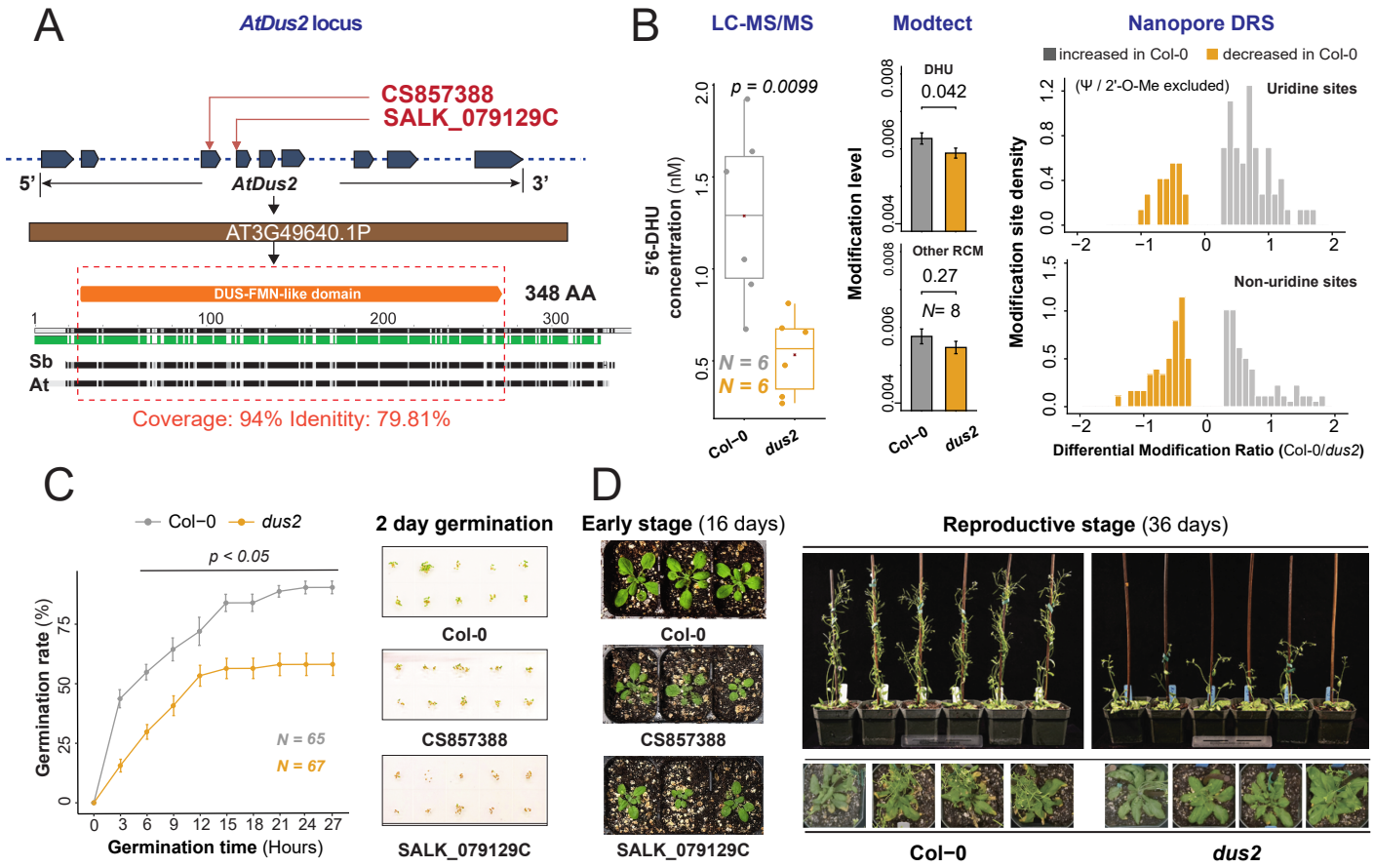
A
AtDus2 locus
CS857388
SALK_079129C
5'
AtDus2
3'
AT3G49640.1P
DUS-FMN-like domain
348 AA
1
100
200
300
Sb
At
Coverage: 94% Idenitity: 79.81%
B
LC-MS/MS
p = 0.0099
5'6-DHU concentration (nM)
N = 6
N = 6
Col−0
dus2
Modtect
Modification level
DHU
0.042
Other RCM
0.27
N= 8
Nanopore DRS
increased in Col-0
decreased in Col-0
(Ψ / 2'-O-Me excluded)
Uridine sites
Non-uridine sites
Modification site density
Differential Modification Ratio (Col-0/dus2)
C
Col−0
dus2
p < 0.05
Germination rate (%)
N = 65
N = 67
Germination time (Hours)
2 day germination
Col-0
CS857388
SALK_079129C
D
Early stage (16 days)
Col-0
CS857388
SALK_079129C
Reproductive stage (36 days)
Col−0
dus2

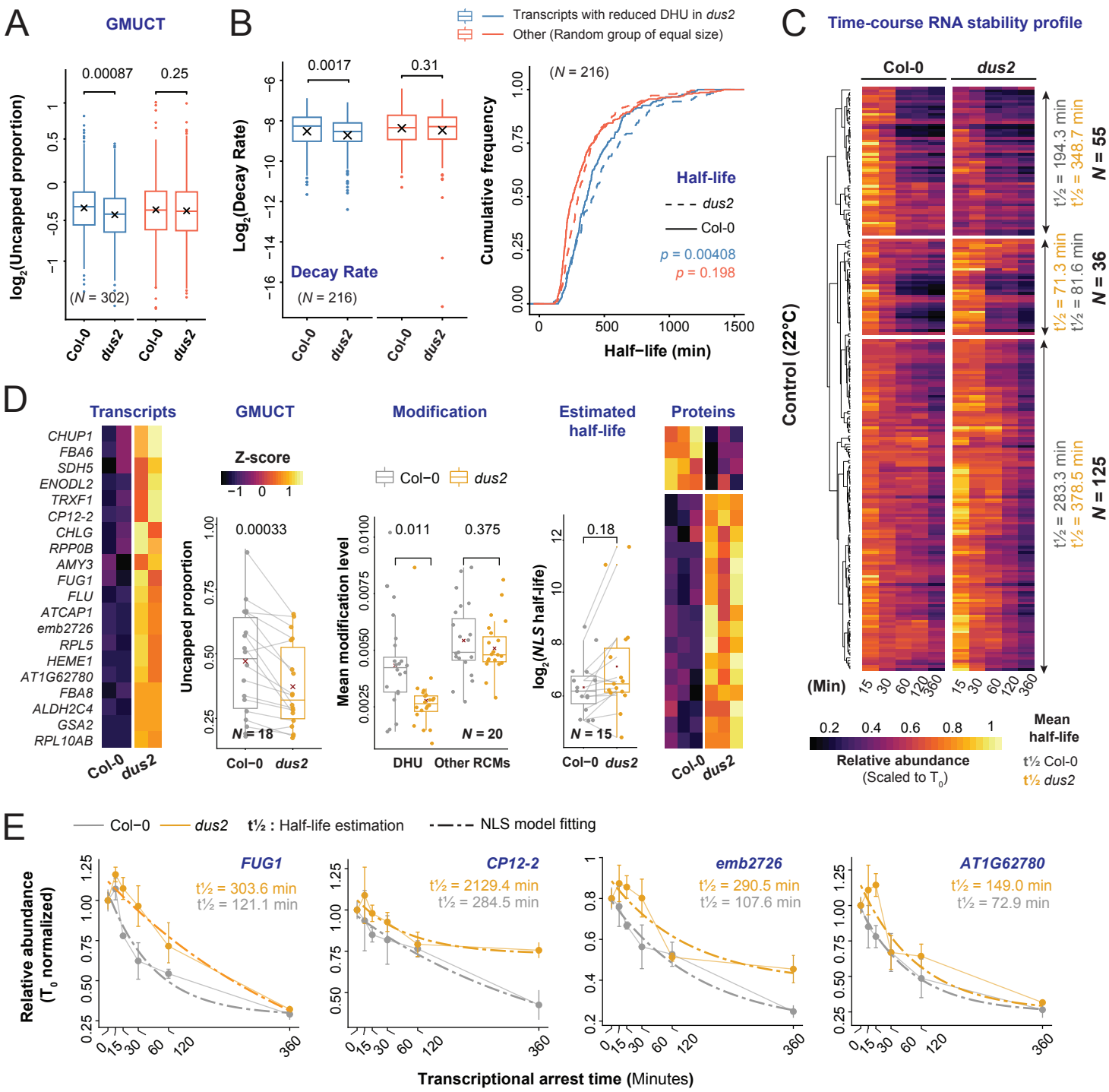
A
GMUCT
0.00087
0.25
log2(Uncapped proportion)
(N = 302)
Col-0
dus2
B
Transcripts with reduced DHU in dus2
Other (Random group of equal size)
0.0017
0.31
Log2(Decay Rate)
Decay Rate
(N = 216)
(N = 216)
Cumulative frequency
Half-life
dus2
Col-0
p = 0.00408
p = 0.198
Half−life (min)
C
Time-course RNA stability profile
Col-0
dus2
Control (22°C)
t½ = 194.3 min
t½ = 348.7 min
N = 55
t½ = 71.3 min
t½ = 81.6 min
N = 36
t½ = 283.3 min
t½ = 378.5 min
N = 125
(Min)
Relative abundance
(Scaled to T0)
Mean half-life
t½ Col-0
t½ dus2
D
Transcripts
GMUCT
Modification
Estimated half-life
Proteins
CHUP1
FBA6
SDH5
ENODL2
TRXF1
CP12-2
CHLG
RPP0B
AMY3
FUG1
FLU
ATCAP1
emb2726
RPL5
HEME1
AT1G62780
FBA8
ALDH2C4
GSA2
RPL10AB
Z-score
Col−0
dus2
0.00033
Uncapped proportion
N = 18
0.011
0.375
Mean modification level
N = 20
DHU
Other RCMs
0.18
log2(NLS half-life)
N = 15
E
Col−0
dus2
t½ : Half-life estimation
NLS model fitting
FUG1
t½ = 303.6 min
t½ = 121.1 min
CP12-2
t½ = 2129.4 min
t½ = 284.5 min
emb2726
t½ = 290.5 min
t½ = 107.6 min
AT1G62780
t½ = 149.0 min
t½ = 72.9 min
Relative abundance
(T0 normalized)
Transcriptional arrest time (Minutes)

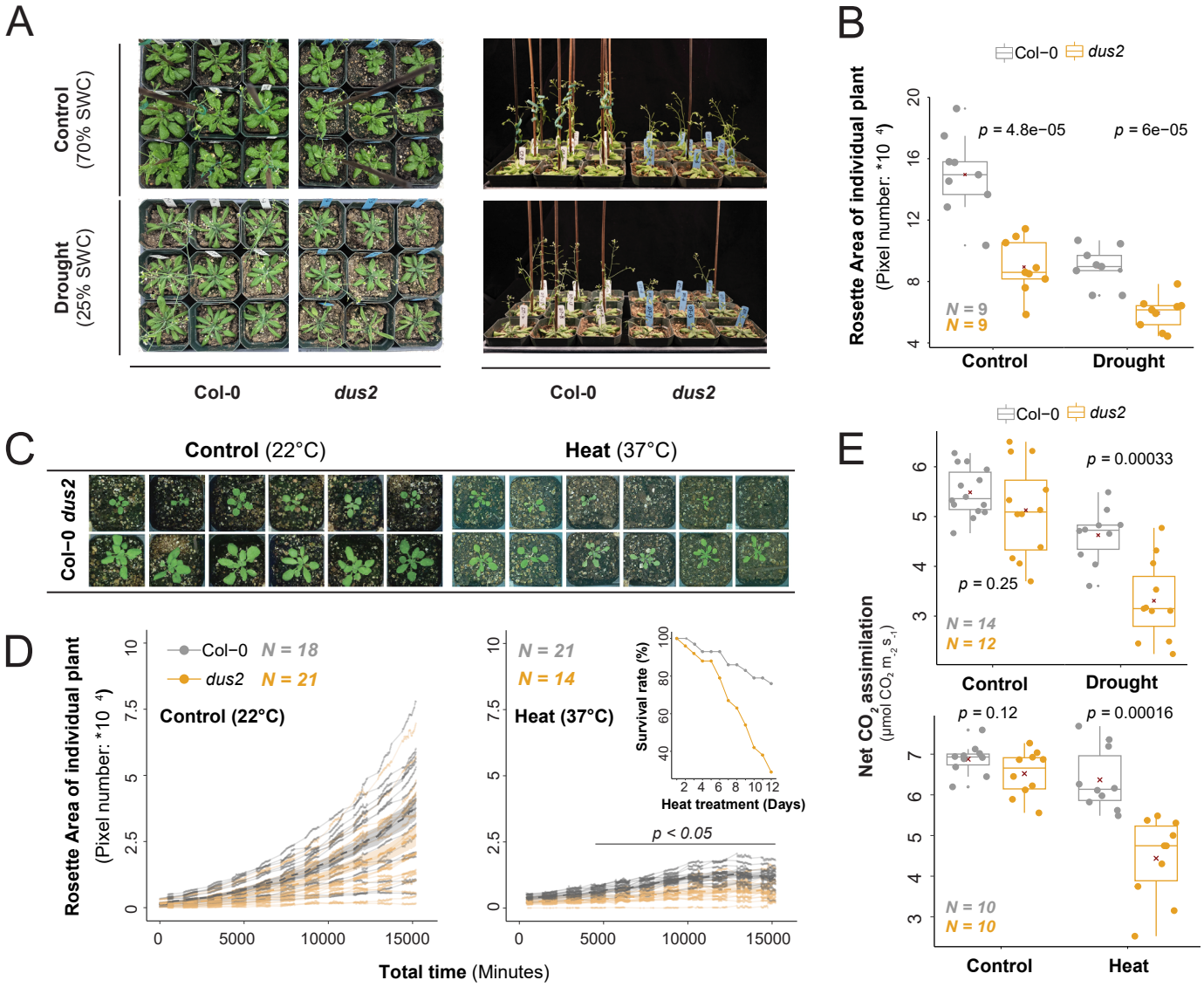
A
Control (70% SWC)
Drought (25% SWC)
Col-0
dus2
Col-0
dus2
B
Col−0
dus2
Rosette Area of individual plant (Pixel number: *10 4)
p = 4.8e−05
p = 6e−05
N = 9
N = 9
Control
Drought
C
Control (22°C)
Heat (37°C)
Col−0
dus2
D
Col−0 N = 18
dus2 N = 21
Control (22°C)
N = 21
N = 14
Heat (37°C)
Survival rate (%)
Heat treatment (Days)
p < 0.05
Rosette Area of individual plant (Pixel number: *10 4)
Total time (Minutes)
E
Col−0
dus2
p = 0.00033
p = 0.25
N = 14
N = 12
Control
Drought
p = 0.12
p = 0.00016
N = 10
N = 10
Control
Heat
Net CO2 assimilation (µmol CO2 m-2 s-1)

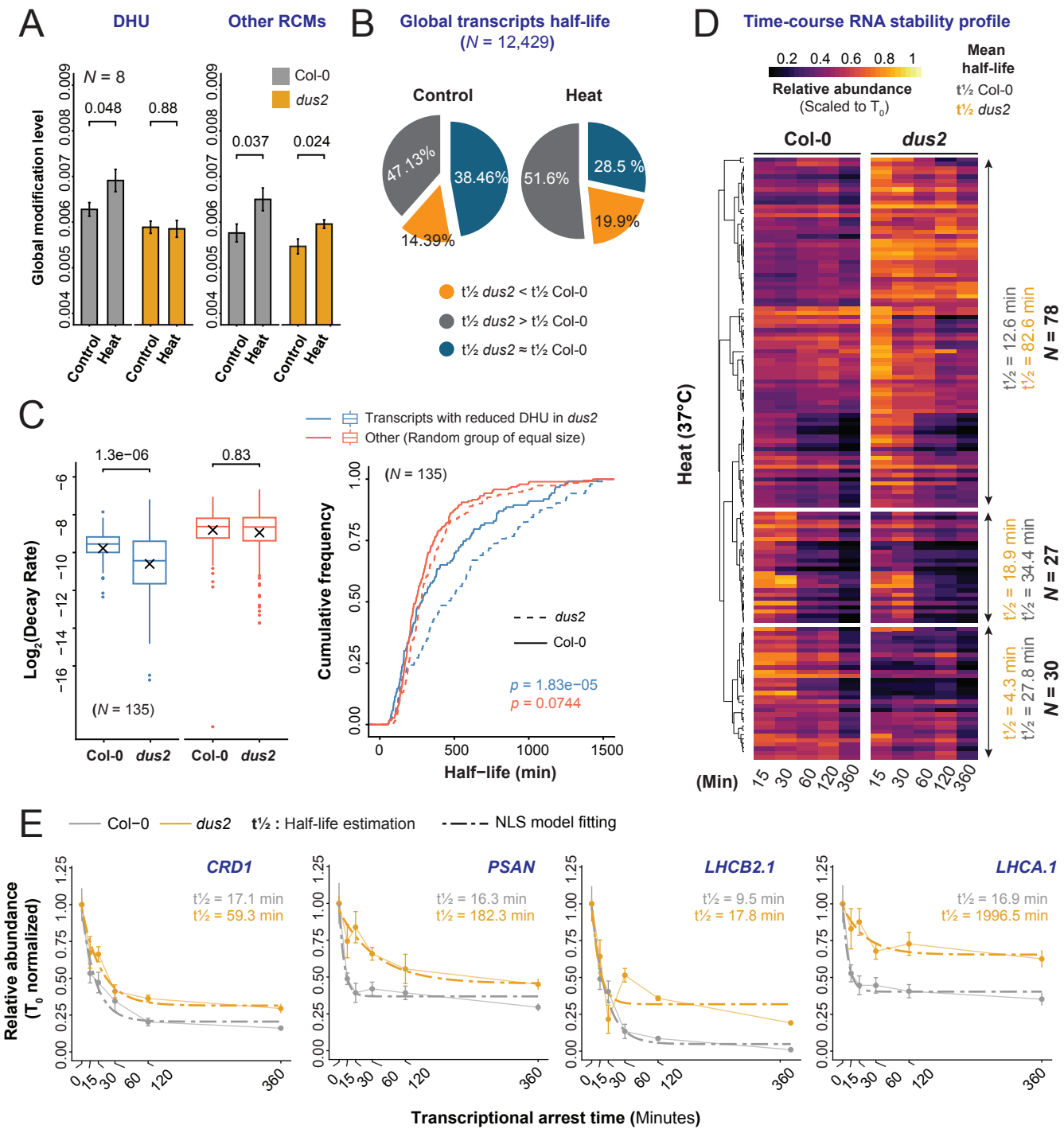
A
DHU
Other RCMs
N = 8
Col-0
dus2
Global modification level
0.048
0.88
0.037
0.024
Control
Heat
B
Global transcripts half-life
(N = 12,429)
Control
Heat
47.13%
38.46%
14.39%
51.6%
28.5 %
19.9%
t½ dus2 < t½ Col-0
t½ dus2 > t½ Col-0
t½ dus2 ≈ t½ Col-0
C
Transcripts with reduced DHU in dus2
Other (Random group of equal size)
1.3e−06
0.83
Log2(Decay Rate)
(N = 135)
Col-0
dus2
Cumulative frequency
(N = 135)
dus2
Col-0
p = 1.83e−05
p = 0.0744
Half−life (min)
D
Time-course RNA stability profile
Relative abundance
(Scaled to T0)
Mean half-life
t½ Col-0
t½ dus2
Col-0
dus2
Heat (37°C)
t½ = 12.6 min
t½ = 82.6 min
N = 78
t½ = 18.9 min
t½ = 34.4 min
N = 27
t½ = 4.3 min
t½ = 27.8 min
N = 30
(Min)
15
30
60
120
360
E
Col−0
dus2
t½ : Half-life estimation
NLS model fitting
Relative abundance
(T0 normalized)
CRD1
t½ = 17.1 min
t½ = 59.3 min
PSAN
t½ = 16.3 min
t½ = 182.3 min
LHCB2.1
t½ = 9.5 min
t½ = 17.8 min
LHCA.1
t½ = 16.9 min
t½ = 1996.5 min
Transcriptional arrest time (Minutes)

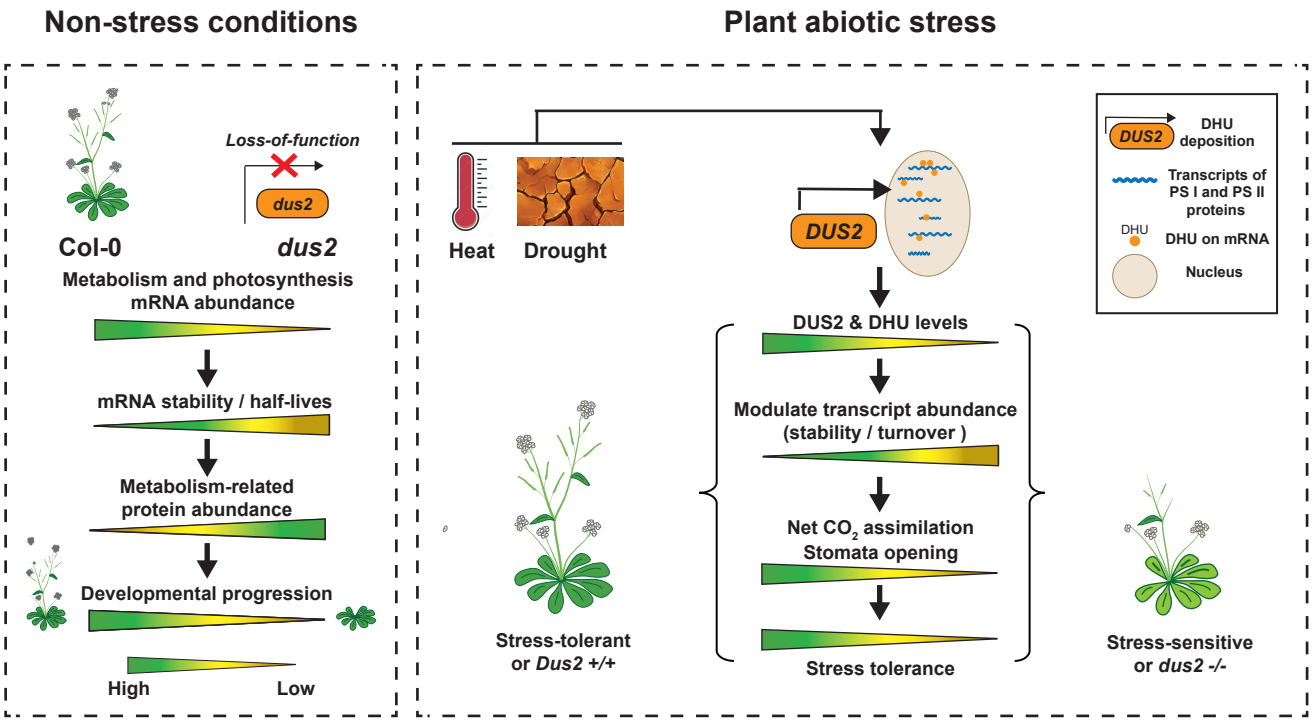
Non-stress conditions
Plant abiotic stress
Loss-of-function
dus2
Col-0
dus2
Metabolism and photosynthesis mRNA abundance
mRNA stability / half-lives
Metabolism-related protein abundance
Developmental progression
High
Low
Heat
Drought
DUS2
DUS2 & DHU levels
Modulate transcript abundance (stability / turnover)
Net CO_2 assimilation
Stomata opening
Stress tolerance
Stress-tolerant or Dus2 +/+
Stress-sensitive or dus2 -/-
DUS2
DHU deposition
Transcripts of PS I and PS II proteins
DHU
DHU on mRNA
Nucleus